

Journal Pre-proof

De novo design approaches targeting an envelope protein pocket to identify small molecules against dengue virus

Emilse S. Leal, Natalia S. Adler, Gabriela A. Fernández, Leopoldo G. Gebhard, Leandro Battini, Maria G. Aucar, Mariela Videla, María Eugenia Monge, Alejandro Hernández de los Ríos, John Alejandro Acosta Dávila, María L. Morell, Sandra M. Cordo, Cybele C. García, Andrea V. Gamarnik, Claudio N. Cavasotto, Mariela Bollini



PII: S0223-5234(19)30762-7

DOI: <https://doi.org/10.1016/j.ejmech.2019.111628>

Reference: EJMECH 111628

To appear in: *European Journal of Medicinal Chemistry*

Received Date: 16 May 2019

Revised Date: 3 August 2019

Accepted Date: 14 August 2019

Please cite this article as: E.S. Leal, N.S. Adler, G.A. Fernández, L.G. Gebhard, L. Battini, M.G. Aucar, M. Videla, Mari. Eugenia. Monge, A. Hernández de los Ríos, J.A. Acosta Dávila, Mari. L. Morell, S.M. Cordo, C.C. García, A.V. Gamarnik, C.N. Cavasotto, M. Bollini, De novo design approaches targeting an envelope protein pocket to identify small molecules against dengue virus, *European Journal of Medicinal Chemistry* (2019), doi: <https://doi.org/10.1016/j.ejmech.2019.111628>.

This is a PDF file of an article that has undergone enhancements after acceptance, such as the addition of a cover page and metadata, and formatting for readability, but it is not yet the definitive version of record. This version will undergo additional copyediting, typesetting and review before it is published in its final form, but we are providing this version to give early visibility of the article. Please note that, during the production process, errors may be discovered which could affect the content, and all legal disclaimers that apply to the journal pertain.

© 2019 Published by Elsevier Masson SAS.

De novo design approaches targeting an envelope protein pocket to identify small molecules against dengue virus

Emilse S. Leal^a, Natalia S. Adler^{a,c}, Gabriela A. Fernández^a, Leopoldo G. Gebhard^b, Leandro Battini^a, Maria G. Aucar^c, Mariela Videla^a, María Eugenia Monge^a, Alejandro Hernández de los Ríos^f, John Alejandro Acosta Dávila^f, María L. Morell^f, Sandra M. Cordo^f, Cybele C. García^f, Andrea V. Gamarnik^g, Claudio N. Cavasotto^{c,d,e}, and Mariela Bollini^{a,#}.

^aCentro de Investigaciones en Bionanociencias (CIBION), Consejo Nacional de Investigaciones Científicas y Técnicas (CONICET), Godoy Cruz, 2390 Ciudad Autónoma de Buenos Aires, Argentina.

^bCONICET-Departamento de Ciencia y Tecnología, Universidad Nacional de Quilmes, Roque Sáenz Peña 352, B1876 Bernal, Buenos Aires, Argentina.

^cComputational Drug Design and Molecular Informatics Laboratory, Translational Medicine Research Institute (IIMT), CONICET-Universidad Austral, Pilar-Derqui, Buenos Aires, Argentina.

^dFacultad de Ciencias Biomédicas, y Facultad de Ingeniería, Universidad Austral, Pilar-Derqui, Buenos Aires, Argentina

^eAustral Institute for Artificial Intelligence, Universidad Austral, Pilar-Derqui, Buenos Aires, Argentina.

^fUniversidad de Buenos Aires, Facultad de Ciencias Exactas y Naturales, Departamento de Química Biológica, Laboratorio de Estrategias Antivirales. CONICET, Instituto de Química Biológica (IQUIBICEN), Buenos Aires, Argentina.

[§]Fundación Instituto Leloir-CONICET, Av. Patricias Argentinas 435, Ciudad Autónoma de Buenos Aires, Argentina Buenos Aires, Argentina.

[#]Correponding author: mariela.bollini@conicet.cibion.

Journal Pre-proof

Abstract

Dengue fever is a mosquito-borne viral disease that has become a major public health concern worldwide. This disease presents with a wide range of clinical manifestations, from a mild cold-like illness to the more serious hemorrhagic dengue fever and dengue shock syndrome. Currently, neither an approved drug nor an effective vaccine for the treatment are available to fight the disease.

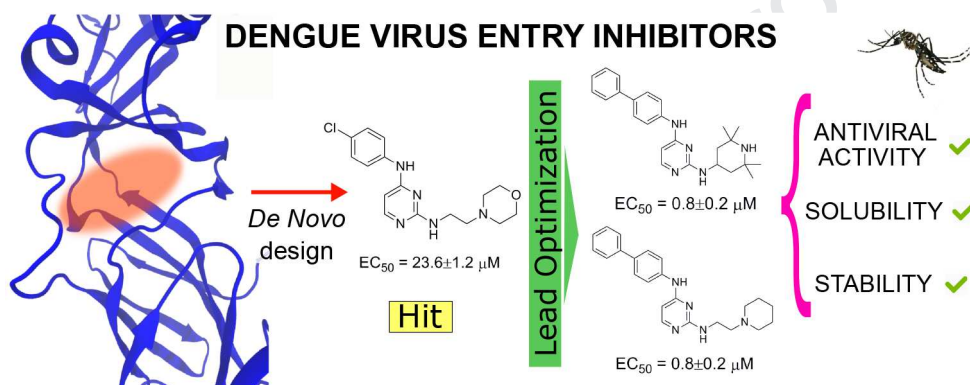
The envelope protein (E) is a major component of the virion surface. This protein plays a key role during the viral entry process, constituting an attractive target for the development of antiviral drugs. The crystal structure of the E protein reveals the existence of a hydrophobic pocket occupied by the detergent *n*-octyl- β -d-glucoside (β -OG). This pocket lies at the hinge region between domains I and II and is important for the low pH-triggered conformational rearrangement required for the fusion of the virion with the host's cell. Aiming at the design of novel molecules which bind to E and act as virus entry inhibitors, we undertook a *de novo* design approach by "growing" molecules inside the hydrophobic site (β -OG). From more than 240000 small-molecules generated, the 2,4 pyrimidine scaffold was selected as the best candidate, from which one synthesized compound displayed micromolar activity. Molecular dynamics-based optimization was performed on this hit, and thirty derivatives were designed *in silico*, synthesized and evaluated on their capacity to inhibit dengue virus entry into the host cell. Four compounds were found to be potent antiviral compounds in the low-micromolar range. The assessment of drug-like physicochemical and *in vitro* pharmacokinetic properties revealed that compounds **3e** and **3h** presented acceptable solubility values and were stable in mouse plasma, simulated gastric fluid, simulated intestinal fluid, and phosphate buffered saline solution.

Keywords *De novo* design, molecular dynamics, anti-dengue virus compounds, pharmacokinetics *in vitro* properties

Highlights

- *De novo* design approach was used to identify new compounds against DENV E protein
- Lead Optimization was performed via molecular dynamics
- Several compounds displayed excellent potency against DENV
- Compounds **3e** and **3h** were potent compounds of all four sero-types of DENV
- **3e** and **3h** showed acceptable *in vitro* pharmacokinetics profile.

Graphical Abstract



1. Introduction

Dengue fever is the most prevalent mosquito-borne viral disease and has become a major public health concern worldwide in recent years. Dengue virus (DENV) belongs to the genus *Flavivirus* (*Flaviviridae*), which are positive-sense single-stranded RNA genome viruses, as several other human pathogens such as West Nile, Japanese encephalitis and Zika viruses [1–3]. To date, four serotypes of DENV have been described, i.e., DENV1 to DENV4. At present, DENV is endemic in more than 100 countries worldwide [4]. The Americas, South-East Asia and Western Pacific are the most seriously affected regions. During 2016 serious outbreaks occurred worldwide, with more than 2.3 million cases being reported in the Americas [5,6].

Controlling DENV epidemic outbreaks remains difficult. Dengue vaccine (Dengvaxia) developed by Sanofi Pasteur has been listed in more than 10 countries to prevent dengue fever [7–9]. However, vaccination requires a three-dose regimen that is limited to individuals aged 9–45 years old, and in seronegative individuals provides modest protection [10]. Currently, there is still no specific antiviral to fight the disease. Although some drugs have been proposed for different DENV proteins, such as the viral polymerase and protease, none of them have been approved [10,11].

The entry of viruses into the host cell is an early and specific stage of infection of which different viral or cellular targets are sensitive to therapeutic intervention. The entry of DENV is initiated by the binding of the viral particle to receptors on the host cell's plasma membrane, followed by internalization via receptor-mediated endocytosis of the virion into the cytosol. The acidic conditions of the endosome compartment trigger a conformational rearrangement of the viral envelope proteins (E) which induces the fusion of the viral and endosomal membranes creating a pore through which the viral genome is released into the host cell's cytoplasm [12,13]. The crystal structure of

DENV-2 E protein reveals a hydrophobic pocket occupied by the detergent *n*-octyl- β -D-glucoside (β -OG). This pocket lies at the hinge region between domains I and II of the E protein. The β -OG pocket is the region where the major conformational changes occur during membrane fusion. Several authors have proposed that small molecules interacting with the E protein can block viral entry. [13–15] The best pharmacological evidence for the pocket as a suitable target was published by Wispelaere *et al.* The authors demonstrated that pyrimidines analogs can bind extracellularly to the E protein, and prevent the infection by blocking E-mediated membrane fusion during viral entry. A resistance mutation, M196V, located adjacent to the β -OG pocket, reduces the affinity and viral infectivity of the evaluated compound [14]. The aim of this work was to identify new molecules that would bind to the β -OG pocket and inhibit DENV entry. To this end, a *de novo* design strategy was employed and the selected compound showed viral inhibition at micromolar concentrations. Through a lead optimization process, several optimized derivatives were obtained which displayed high improvement in the antiviral activity and pharmacokinetics *in vitro* properties (solubility, logP, and stability).

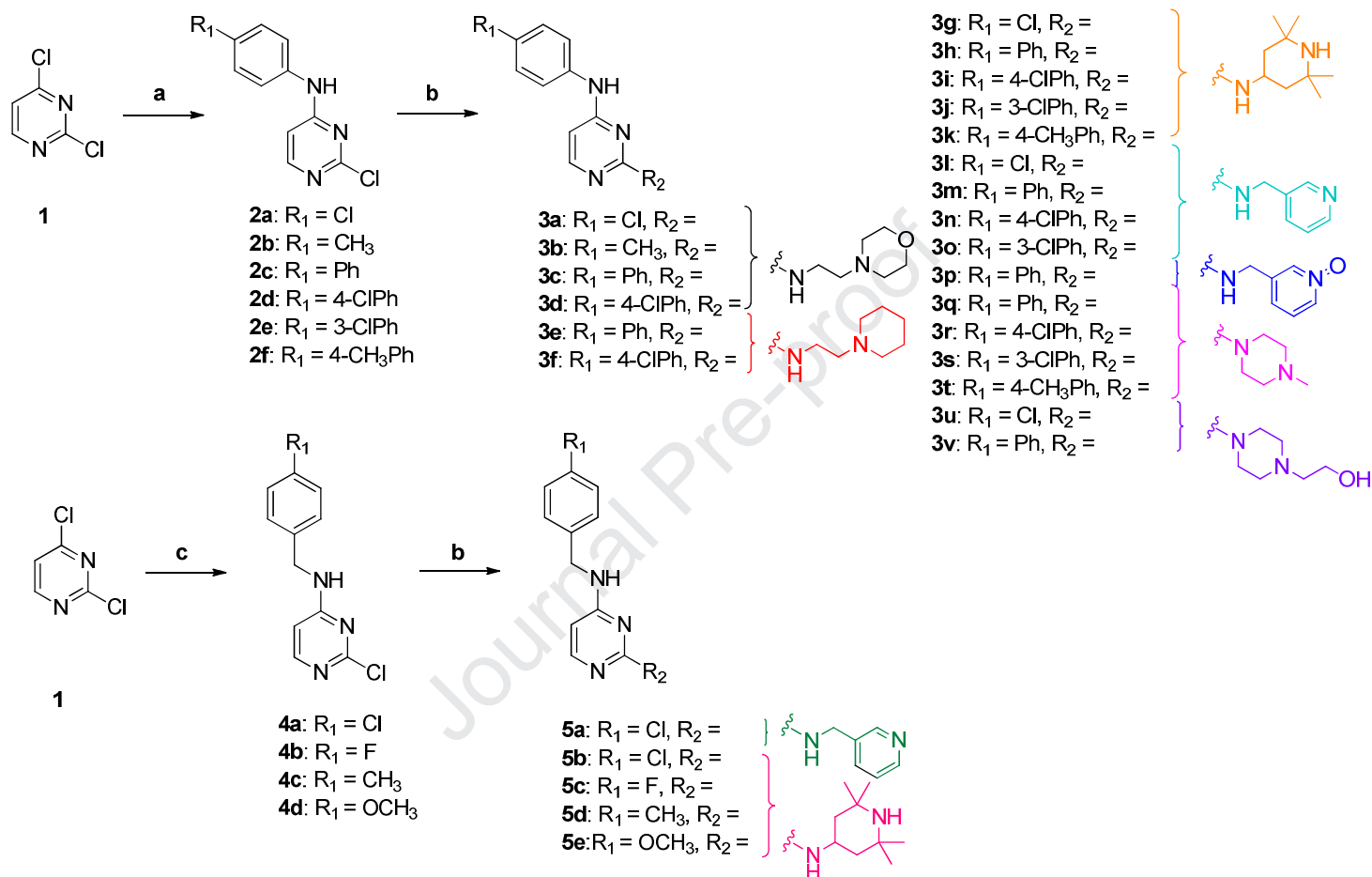
2. Results and discussion

2.1. Chemistry

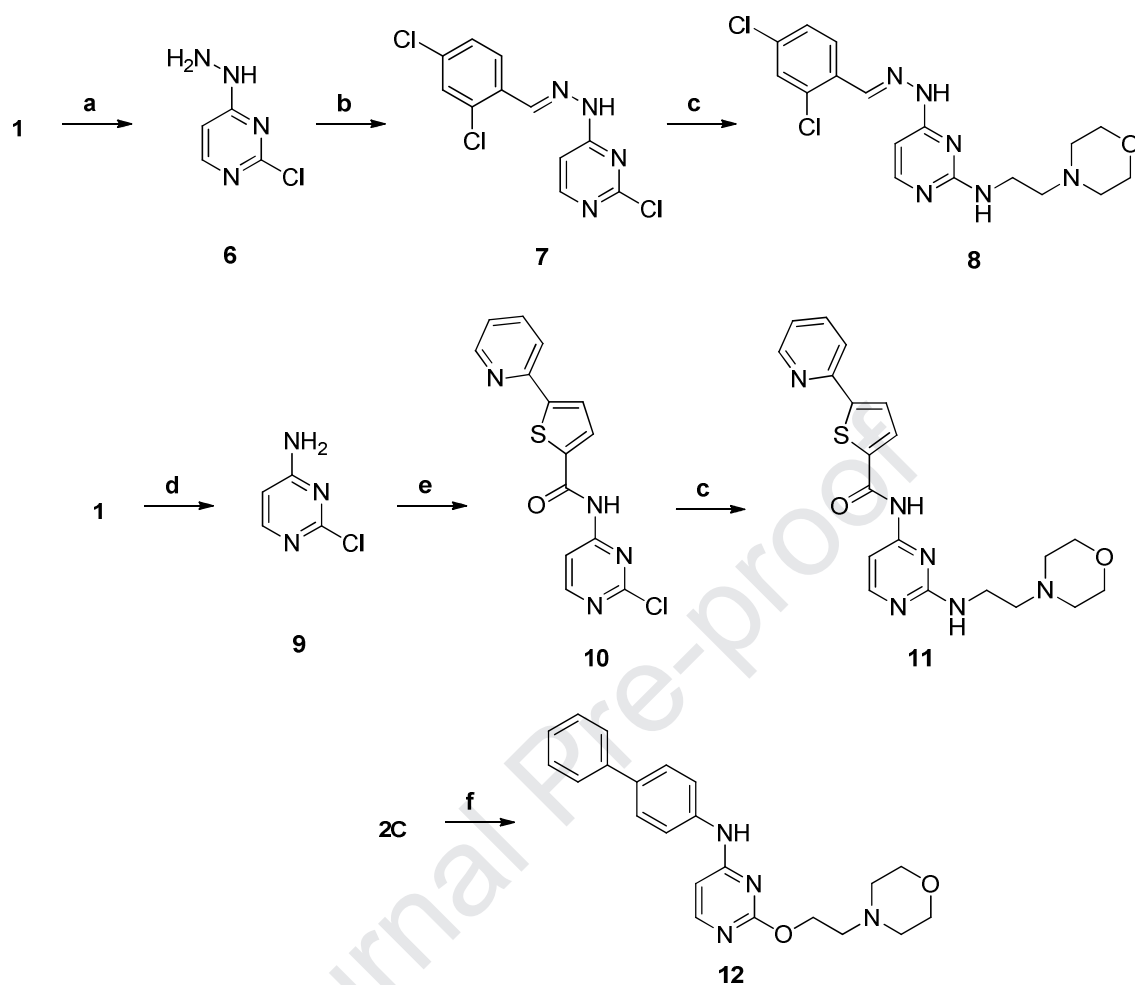
On the basis of the *de novo* design considerations (section 2.3), we prepared a range of 2,4-disubstituted pyrimidine analogs (Scheme 1). The synthesis of pyrimidine analogs was based on previously described procedures [16]. The desired compounds were obtained through a S_NAr reaction of anilines and amines with heteroaryl chlorides [17]. Compounds **2a-f** and **4a-d** were obtained in high yield by selective substitution in position 4 with commercially available or synthesized anilines and benzylamines in the presence of DIPEA in *n*-butanol (**2a-f**) or ethanol (**4a-d**). Finally, the desired

compounds (**3a-v** and **5a-e**) were prepared through a S_NAr from monosubstituted pyrimidine, (**2a-f** and **4a-d**) and the corresponding alkyl amines. Due to the lack of reactivity of the 2-position of *N*-4-pyrimidine derivatives, the reaction was carried out in sealed tube at reflux with a low yield.

Compound **8**, **11** and **12** were obtained as shown in scheme 2. The intermediate hydrazone (**7**) was obtained by the condensation of 4-hydrazino-2-chloro pyrimidine (**6**) with 2,4-dichlorobenzaldehyde. Compound **10** was prepared by the condensation of 5-(pyridin-2-yl)thiophene-2-carboxylic acid and 2-chloropyrimidin-4-amine, in the presence of EDCI.HCl and HOBT in NMP. Compound **12** was prepared via a S_NAr reaction of the compound (**2c**) with a sodium alkoxide in THF.



Scheme 1. General procedure for synthesis of compounds **3a-v** and **5a-e**. Reagents and conditions (a) Amines, DIPEA, *n*-butanol, 110°C, overnight. (b) Amines, DIPEA, *n*-butanol, 190°C, sealed vial. (c) Benzylamines, DIPEA, ethanol, 90°C, overnight.



Scheme 2. Synthesis of compounds **8**, **11** and **12**. Reagents and conditions (a) NH_2NH_2 , TEA, methanol, rt, 2 h. (b) 2,4-Dichlorobenzaldehyde, ethanol, reflux, 1 h. (c) 4-(2-Aminoethyl)morpholine, DIPEA, 190°C , sealed vial. (d) NH_4OH , 90°C , 5 h. (e) 5-(Pyridin-2-yl)thiophene-2-carboxylic acid, EDCI·HCl, HOBt, NMP, rt, overnight, (f) 4-(2-Hydroxyethyl)morpholine, NaH, THF, 80°C , overnight.

2.2. Antiviral activity

The antiviral activity was evaluated for each newly designed compounds monitoring the expression of the luciferase from a recombinant fully functional reporter infectious DENV-2 bearing a luciferase coding sequence. [18,19] After infection of cells in culture

with the reporter DENV, the luciferase activity peaks at 8 h as a result of the translation of the incoming viral genome. Thus, luciferase activity at this time point reflects entry of the reporter virus. After 24 h post-infection, the genome amplification by the viral polymerase occurs, leading to an increase in the luciferase activity, which accounts for the synthesis of viral RNA. The luciferase activity was measured at 8 h post-infection with the reporter DENV in either untreated control and in cells treated with each of the thirty compounds synthesized (Tables 1 and 2). Two of the active inhibitors, that block an early infection step, were further evaluated for their antiviral activity against fully DENV1-4 infectious viral particles by a virus yield inhibition assay [20]. Cells were infected at a multiplicity of infection (m.o.i.) of 0.1 plaque formation units per cell (PFU/cell) and further incubated in the presence of different compound concentrations during 24 and 48 h. Virus replication was inhibited by both compounds in a dose-dependent manner attaining a reduction higher than 50% in virus titres in the range of concentrations 0.3-1.5 μ M for all DENV serotypes (Table 3).

In parallel to antiviral activity, cell viability was measured after the treatment with different concentrations of each compound using cristal violet and the 3-(4,5-dimethylthiazol-2yl)-2,5-diphenyl tetrazolium bromide (MTT) assay, as described previously[21].

2.3. *De novo* design of DENV E protein inhibitors

Taking into account the crystal structure of the binding site occupied by β -OG reported by Modis *et al.* [22], we designed new small organic molecules with the capacity to bind the E protein like the β -OG ligand. The β -OG pocket entrance contains some hydrophilic amino acid residues that could establish electrostatically favorable interactions with ligands (for example, Thr48, Glu49, Gln200, Gln271, and Thr280). Besides, several polar atoms present at the pocket entrance are suitable partners for

energetically favorable hydrogen bond interactions. The hydrophobic pocket, which is occupied by the *n*-octyl chain of the β -OG ligand in the crystal structure, is large enough to accommodate the hydrophobic groups present in small molecule inhibitors [14,23–27].

Based on the chemical features and critical interactions with the β -OG binding site of the active compounds previously reported [27,28], we generated a virtual chemical library using the BOMB program [29]. The library was grown starting with NH_3 as the core, which was positioned to form a hydrogen bond with the Thr48 carbonyl group. All templates were designed to fulfill these key requirements: (i) to deliver a hydrophobic group into the hydrophobic pocket, as the β -OG octyl chain; (ii) to incorporate an NH to the hydrogen bond with Thr48, and (iii) to incorporate polar substituents into the channel entrance. An extensive conformational search was performed for each ligand; each conformer was optimally positioned and the one with lowest energy was scored as output. The structure optimization was performed with the OPLS-AA force field[30]. The prime parameters for the analysis were the protein-ligand potential energy (E_{PL}), the desolvation energy and surface-area burial for the ligand, and the drug-like predicted properties including solubility and cell permeability [31]. Around 240,000 molecules were then built to form the Phx - NH - Het - U motif, where NH is a core, U is a solubilizing group, Het is a heterocyclic ring, and Phx is a substituted (X) phenyl ring (Ph). The top-25 scoring analogs are dominated by quinazoline and pyrimidine as Het. The top 5-analogs have chlorine at 4- and 5- phenyl position (PhX) and 2-morpholinoethanamine, and piperazine as solubilizing group (U). In the end, we selected compound **3a** based on the high E_{PL} value, adequate drug-like predicted properties and synthetic feasibility compared to the rest of the candidates.

Next, we docked **3a** within the binding site and performed a 100 ns molecular dynamics (MD) simulation to determine the stability of the predicted conformations by BOMB and to explore the putative binding mode of the selected ligands with the E protein. During the first 40 ns of the simulation, **3a** established a hydrogen bond interaction between the N-H at position 4 of the pyrimidine structure and the OH of the Thr280 (Figure 1A). The interatomic distance and the typical hydrogen bond angle were nearly 2 Å and 160°, respectively (Figure S1). After establishing this interaction, the ligand moved slightly from the initial conformation to another conformation that remained stable for the rest of the simulation. No hydrogen bond interactions were detected during that period.

Compound **3a** was synthesized and cytotoxicity was evaluated in A549 cell line. Also, antiviral activity was tested by the luciferase-reporter DENV assay mentioned above [18,19]. This ligand displayed antiviral activity against DENV-2 (EC_{50} 23.6 μ M) and no cytotoxicity was observed at 50 μ M. Although the antiviral activity was moderate, it was considered a good starting point for lead optimization.

2.4. Lead optimization

Initial analogs of 3a. A computer-aided drug optimization was carried out in order to improve the antiviral activity of **3a**. For this purpose, we used a combination of design using the BOMB software followed by docking/MD simulations. In the first step, the determination of the optimal substitution pattern (X) of the Ph scaffold was performed by BOMB. The best E_{PL} scores were obtained by the introduction of voluminous substituents such as X= Ph group. Analogues were the docked within the binding site, followed by 100 ns MD simulations. We were thus able to confirm that the close contacts made by all the ligands and the E protein became stronger and more stable as the size of the X chain increased. Furthermore, the more voluminous ligands also

established stronger and more stable H bond interactions. In particular, the MD simulations of compound **3c** and **3d** revealed that the biphenyl ring group fitted very well in the hydrophobic pocket establishing an energetically favorable hydrophobic contact with Thr48, Val130, Leu135, Met196, Ile270, and Phe279 side chains. In particular, a strong hydrophobic interaction was observed between the terminal aromatic ring of the biphenyl group and Phe193 at a distance of 5 Å. These ligands established stable hydrogen bond interactions with the E protein. Both of them presented a moderate hydrogen bond between the N-H at position 4 of the pyrimidine with the carbonyl O of the Thr48, (interatomic distances of 2.2 Å and a bond angle of 150°) (Figures S2 and S3). At the end of the simulation performed with **3d**, this ligand was found to move slightly from the initial conformation to another conformation that remained stable for the rest of the measurement period, and a new hydrogen bond was formed between the O of the Ala50 and the N-H at position 2 of the pyrimidine. The interatomic distances and H bond angle were 1.9 Å and 160°, respectively (Figure S4).

During the second half of the simulation, another H bond was formed between the N3 of **3c** and **3d** and the backbone amide H of Ala50 (interatomic distance of 2.2 Å and a bond angle of 160°) (Figures S5 and S6). For the entire simulation period, the morpholine group remained exposed to the solvent (Figure 1B). The MD simulations revealed a common pattern of interaction with the β -OG pocket in the E protein, which was in agreement with the interactions predicted by the *de novo* design.

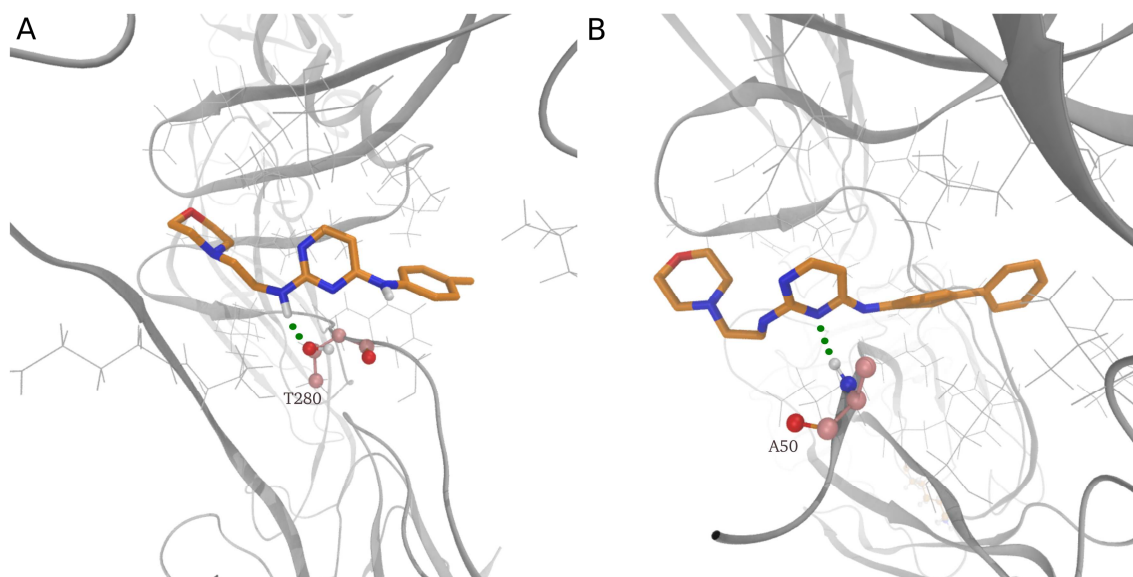
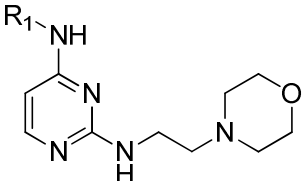
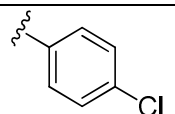
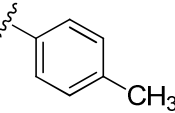
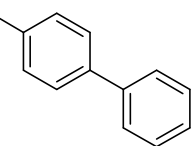
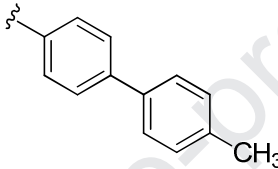
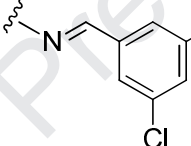
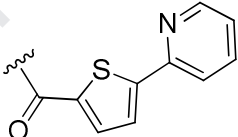
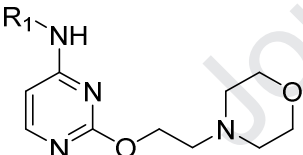
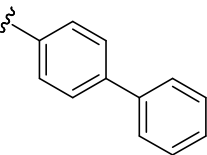


Figure 1. Predicted interaction of active compounds **3a** (A) and **3c** (B) within the E protein binding site (PDB ID 1OKE) obtained by the molecular dynamics simulations.

Based on the outcome of the MD simulations, compounds **3c** and **3d** were synthesized and evaluated in the early infection steps dengue antivirals using an assay that allows discriminating entry/translation and genome amplification. As expected, both compounds were 3- and 13-fold more active than the predecessor **3a**, respectively. The influence of other substituents, at position 4 of the pyrimidine ring on the biological activity was also investigated. Compounds **8** and **11**, whose aromatic rings were found to fit well in the hydrophobic pocket were more active than the reference compound **3a**. (Table 1, Figure S7). In addition, a pairwise comparison of the activities of compounds **3c** and **12** ($EC_{50} = 8.6$ vs. $39.7 \mu\text{M}$) revealed the crucial role of the NH at position 2 of the pyrimidine for the biological activity.

Table 1. Anti-DENV activity and cytotoxicity of compounds **3a-d**, **8**, **11** and **12**.

| Core structure | Compound | R1 | EC ₅₀ (μ M) ^a | CC ₅₀ (μ M) ^b | SI ^d |
|---|-----------|---|---|---|-----------------|
|  | 3a |  | 23.6 \pm 1.2 | 89.6 \pm 2.3 | 4 |
| | 3b |  | 21.3 \pm 1.6 | >50 | >2 |
| | 3c |  | 8.6 \pm 1.1 | 59.0 \pm 1.8 | 7 |
| | 3d |  | 1.8 \pm 1.0 | 10.2 \pm 0.9 | 5 |
| | 8 |  | 10.6 \pm 1.0 | 76.5 \pm 1.8 | 8 |
| | 11 |  | 3.3 \pm 1.8 | 10.5 \pm 1.1 | 4 |
|  | 12 |  | 39.7 \pm 1.1 | ND ^c | ND |

^aEffective concentration 50%: concentration required to achieve a two-fold reduction of luciferase activity compared to control. Results represent the mean from at least two independent experiments analyzed by GraphPad Prism software.

^bCytotoxic concentration 50 is defined as a concentration required to reduce the viability of A549 cells by 50%, as determined by MTT method. Results represent the mean from at least two independent experiments.

^cND: Not determined.

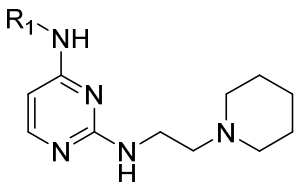
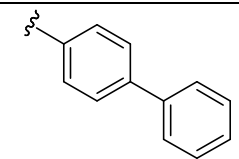
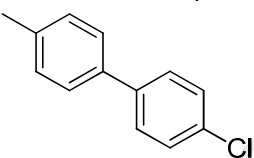
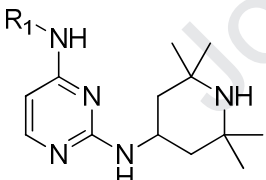
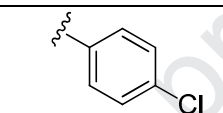
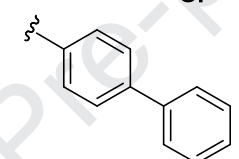
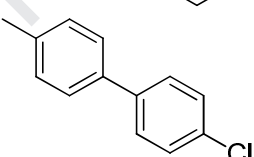
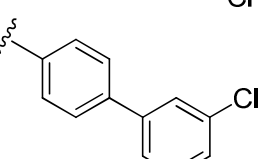
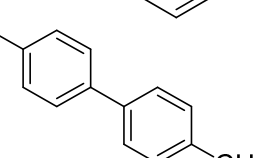
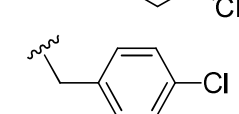
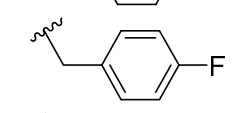
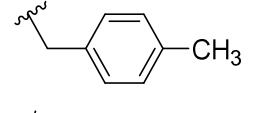
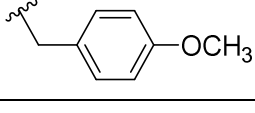
^dSI: selectivity index (SI = CC₅₀/EC₅₀).

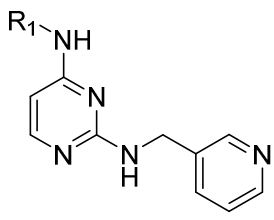
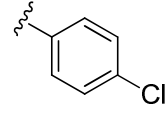
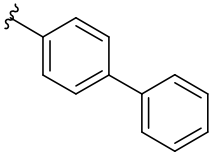
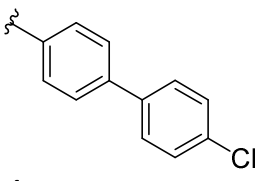
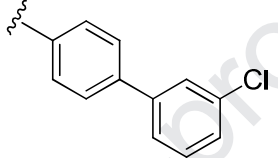
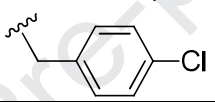
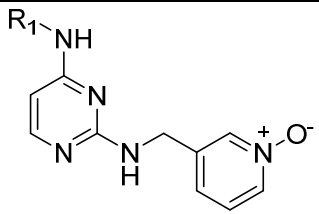
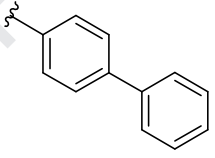
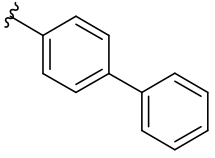
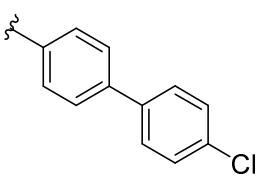
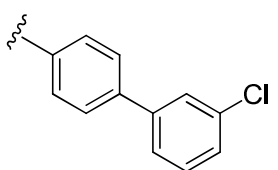
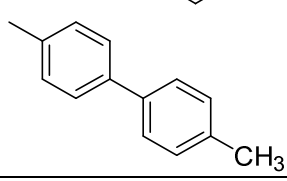
The next step in the study was to evaluate the influence of the terminal heterocyclic ring on the antiviral activity. Therefore, we replaced the ethylmorpholine scaffold of **3a** by ethylpiperidine (**3e**), tetramethylpiperidine (**3h**), methylpyridine (**3m**), methylpyridine *N*-oxide (**3p**), and 4-methyl and *N*-ethanolpiperazine (**3q** and **3v**, respectively). In general, all the compounds were active within the low micromolar range. These results demonstrate that the activity is more dependent on the size of the X chain than on the heterocyclic ring exposed to the solvent. In particular, **3e** and **3h** exhibited higher activity against DENV, as compared to the rest of compounds of the series (**3c**, **3h**, **3m**, **3p**, **3q** and **3v**). (Table 2).

Analogs of 3h. Several **3h** derivatives ($EC_{50}=0.8 \mu\text{M}$) were synthesized and evaluated against DENV. In general, all derivatives exhibited activity in a low micromolar range, including compound **3g**, which bears a *p*-chlorophenyl group at position 4 of the pyrimidine ring ($EC_{50}=1.9 \mu\text{M}$). Compounds **3i** and **3j**, bearing a chlorine atom in *p*- and *m*-position of the biphenyl group, were the most potent compounds of this series, with EC_{50} values of $0.1 \mu\text{M}$ and $0.5 \mu\text{M}$, respectively. These results were also corroborated by measuring intracellular viral RNA level after treatment with the compounds for 48 h post infection (p.i.) by qRT-PCR.

Taking into account the activity of **3g**, the X chain appears to have less influence on the biological activity, as compared to the rest of the series (Tables 1 and 2). Further MD simulations revealed the existence of a stable electrostatic interaction between the NH charged group of the tetramethylpiperidine scaffold and Glu49 (Figure 2). The contribution of this residue to the calculated binding free energy was notably higher than that of the other residues, which explains why the influence of the X chain on the EC_{50} values is diminished.

Table 2. Anti-DENV activity and cytotoxicity of compounds **3e-v** and **5a-e**.

| Core | Compound | R ₁ | EC ₅₀ (μ M) ^a | CC ₅₀ (μ M) ^b | SI ^d |
|---|--|--|---|---|-----------------|
|  | 3e |  | 0.8 \pm 0.2 | 18.1 \pm 1.0 | 23 |
| | 3f |  | 1.1 \pm 0.3 | 14.3 \pm 0.8 | 13 |
|  | 3g |  | 1.90 \pm 1.0 | 18.6 \pm 1.9 | 10 |
| | 3h |  | 0.8 \pm 0.2 | 17.3 \pm 0.8 | 22 |
| | 3i |  | 0.18 \pm 0.1 | 9.8 \pm 1.1 | 54 |
| | 3j |  | 0.54 \pm 0.2 | 5.1 \pm 1.2 | 10 |
| | 3k |  | 1.51 \pm 1.0 | 12.0 \pm 0.7 | 8 |
| | 5b |  | 1.8 \pm 1.1 | 21.1 \pm 1.3 | 12 |
| | 5c |  | 1.98 \pm 1.1 | 12.8 \pm 0.2 | 7 |
| | 5d |  | 4.90 \pm 1.0 | 15.2 \pm 0.5 | 3 |
| 5e |  | 12.5 \pm 0.9 | 18.3 \pm 1.2 | 2 | |

| Core | Compound | R1 | EC ₅₀ (μ M) ^a | CC ₅₀ (μ M) ^b | SI ^d |
|---|-----------|--|---|---|-----------------|
|  | 3l |  | 24.0 \pm 1.1 | ND ^c | ND |
| | 3m |  | 7.4 \pm 1.0 | 40 \pm 1.2 | 5 |
| | 3n |  | 4.1 \pm 1.1 | 25.7 \pm 1.2 | 6 |
| | 3o |  | 3.4 \pm 1.1 | 18.5 \pm 1.9 | 5 |
| | 5a |  | 23.7 \pm 1.6 | ND | ND |
|  | 3p |  | 9.1 \pm 1.0 | 30.2 \pm 1.5 | 3 |
| | 3q |  | 4.6 \pm 0.9 | 25.1 \pm 1.2 | 5 |
| | 3r |  | 3.3 \pm 0.9 | 23.5 \pm 1.2 | 5 |
| | 3s |  | 2.9 \pm 1.1 | 15.3 \pm 0.8 | 5 |
| | 3t |  | 4.9 \pm 1.2 | 27.7 \pm 1.0 | 6 |

| Core | Compound | R1 | EC ₅₀ (μ M) ^a | CC ₅₀ (μ M) ^b | SI ^d |
|------|-----------|----|---|---|-----------------|
| | 3u | | 24.0 \pm 1.1 | ND | ND |
| | 3v | | 19.9 \pm 1.3 | ND | ND |

^aEffective concentration 50%: concentration required to achieve a two-fold reduction of luciferase activity compared to control. Results represent the mean from at least two independent experiments analyzed by GraphPad Prism software.

^bCytotoxic concentration 50 is defined as a concentration required to reduce the viability of A549 cells by 50%, as determined by MTT method. Results represent the mean from at least two independent experiments.

^cND: Not determined.

^dSI: selectivity index ($SI = CC_{50}/EC_{50}$).

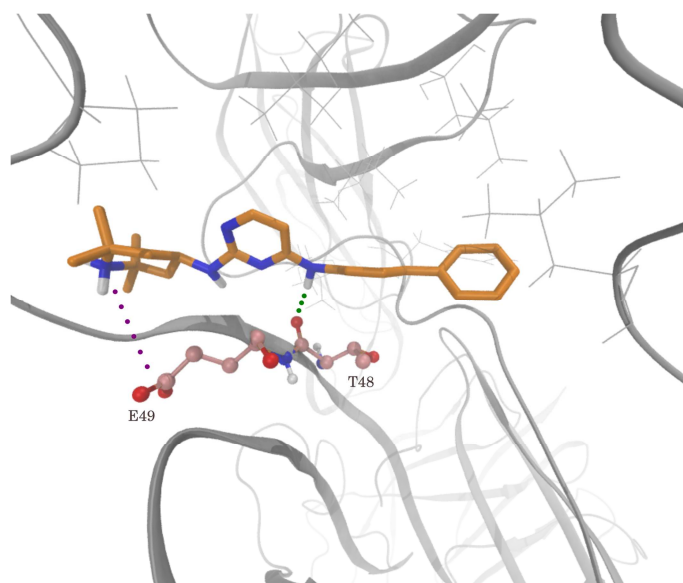


Figure 2. Predicted interaction of compound **3h** within the *E* protein β -OG binding site, obtained by molecular dynamics simulation. The electrostatic interaction and hydrogen bond are shown as violet and green dashed lines respectively.

Since all DENV serotypes co-circulate simultaneously in several tropical and subtropical areas, the antiviral activity against infectious virus particles of serotypes 1-4 was further evaluated. Based on the high conservation of the residues involved in the interaction between protein E and ligands, we expected active compounds to display antiviral activity against the four serotypes of DENV. Compounds **3e** and **3h** were selected for evaluation because they presented high potency and better calculated physicochemical properties (solubility, clogP). As expected, both compounds were found to be active against the four DENV serotypes, with slight differences between serotypes (Table 3).

Table 3. Antiviral activity profile of **3e** and **3h** against DENV serotypes.

| Compound | EC ₅₀ (μM) ^a | | | |
|-----------|------------------------------------|----------|----------|----------|
| | DENV-1 | DENV-2 | DENV-3 | DENV-4 |
| 3e | 0.87±0.1 | 0.85±0.2 | 0.56±0.2 | 2.5±1.1 |
| 3h | 0.58±0.1 | 0.81±0.2 | 0.39±0.8 | 0.87±0.3 |

^aEffective concentration 50% (EC₅₀) was calculated as the concentration required to reduce virus yield by 50% in the compound - treated cell cultures compared with untreated ones at 48 h p.i. All determinations were performed in triplicate. Values represent the mean ± standard deviation from triplicate independent tests.

2.5 Physicochemical and *in vitro* pharmacokinetic properties of the selected compounds

The physicochemical properties of the most promising compounds (**3e** and **3h**) were evaluated *in vitro* in terms of solubility and stability. The solubility was tested at three different pH values (1.2, 6.8, and 7.4) employing the shake-flask method [32]. Solubility data are summarized in Table 3. All compounds presented acceptable solubility values, which were within the range normally observed for oral drugs, i.e., 4-4000 μg/mL (corresponding to S values ranging from 10⁻² to 10⁻⁵ M for compounds with a molecular weight of 400) [33]. The clogP values for the listed compounds ranged from 3 to 5, which are also within the range for oral drugs (0-5) [34]. Stability studies were conducted in PBS (pH 7.4), simulated intestinal fluid (SIF, pH 6.8), simulated gastric fluid (SGF, pH 1.2), and mouse plasma and both compounds were proven to be stable under all evaluated conditions.

Table 4. Physicochemical and pharmacokinetics *in vitro* properties for **3e** and **3h**.

| Cmpd | Solubility ($\mu\text{g/mL}$) ^a | | | ^b cLogP | $t_{1/2}$ (min) ^c | | | Plasma |
|-----------|--|--------------|------------|--------------------|------------------------------|----------|----------|--------|
| | SGF | SIF | PBS | | SGF | SIF | PBS | |
| | (pH 1.2) | (pH 6.8) | (pH 7.4) | | (pH 1.2) | (pH 6.8) | (pH 7.4) | |
| 3e | 506 \pm 17 | 324 \pm 29 | 32 \pm 6 | 4.7 | > 120 | > 120 | > 120 | > 120 |
| 3h | 76 \pm 10 | 580 \pm 49 | 93 \pm 6 | 5.0 | > 120 | > 120 | > 120 | > 120 |

^aExperimental solubility at pH 1.2, 6.4 and 7.4. Values are expressed as the mean \pm standard deviation of two independent experiments run in triplicate.

^bcLog P: Predicted by the Qikprop software. [35]

^cSGF, SIF, PBS and mouse plasma stability

3. Conclusions

On the basis of our hit identification and lead optimization strategy, thirty new molecules were synthesized. Four of the new derivatives displayed significant anti-DENV activity ($\text{EC}_{50} < 1 \mu\text{M}$) targeting the early steps of viral infection. Two of the most promising compounds (**3e** and **3h**) proved to be active against the four DENV serotypes. Both compounds showed adequate solubility and high stability profiles in different media. Taking all this into account we consider that the pyrimidine analogs are a good starting point for the development of novel antivirals against DENV infection.

4. Experimental section

4.1. Chemistry

Column chromatography was carried out employing Merck silica gel (Kieselgel 60, 63-200 μm). Precoated silica gel plates F-254 were used for thin-layer analytical

chromatography. NMR spectra were recorded on Bruker Biospin 600 MHz AVIII600, Bruker advance II 500 MHz and Bruker 300 MHz spectrometers at room temperature. Chemical shifts (δ) are reported in ppm and coupling constants (J) in Hertz. The mass spectrometer utilized was a Xevo G2S QTOF (Waters Corporation, Manchester, UK) with an electrospray ionization (ESI) source. The mass spectrometer was operated in positive and negative ion modes with probe capillary voltages of 2.5 and 2.3 kV, respectively. The sampling cone voltage was 30 V. The source and desolvation gas temperatures were set to 120 and 350 °C, respectively. The nitrogen gas desolvation flow rate was 600 L h⁻¹ and the cone desolvation flow rate was 10 L h⁻¹. The mass spectrometer was calibrated across the range of m/z 50–1200 using a 0.5 mM sodium formate solution prepared in 2-propanol/water (90:10 v/v). Data were drift corrected during acquisition using a leucine enkephalin reference spray (LockSpray) infused at 2 μ L min⁻¹. Data were acquired in the range of m/z 50–1200, and the scan time was set to 1 s. Data acquisition and processing were carried out using MassLynx, version 4.1 (Waters Corp., Milford, MA, USA).

4.1.1. General procedure for synthesis of compounds **2a-f**. To a pressure round-bottom flask containing the mixture of 2,4-dichloropyrimidine (**1**) (2.0 mmol) and the corresponding amine (2.0 mmol) in *n*-butanol (5 mL), DIPEA was added (10.0 mmol) slowly to the solution. The mixture was stirred at 110 °C overnight. The products were obtained as solids, which were filtrated from the reaction mixture and recrystallized from ethanol.

4.1.1.1. 2-chloro-*N*-(4-chlorophenyl)pyrimidin-4-amine (**2a**). Yield: 0.224 g, 46%. ¹H NMR (600 MHz, CDCl₃) δ 8.16 (d, J = 5.9 Hz, 1H), 7.40 – 7.36 (m, 2H), 7.31 – 7.27 (m, 2H), 6.93 (br s, 1H), 6.55 (d, J = 5.9 Hz, 1H).

4.1.1.2. 2-chloro-*N*-(*p*-tolyl)pyrimidin-4-amine (**2b**). Yield: 0.380 g, 87%. ¹H NMR (300 MHz, CDCl₃) δ 8.11 (d, *J* = 5.9 Hz, 1H), 7.25 – 7.16 (m, 4H), 6.95 (s, 1H), 6.54 (d, *J* = 5.9 Hz, 1H), 2.29 (s, 3H).

4.1.1.3 *N*-((1,1'-biphenyl)-4-yl)-2-chloropyrimidin-4-amine (**2c**). Yield: 0.350 g, 53%. ¹H NMR (600 MHz, DMSO-*d*₆) δ 10.14 (s, 1H), 8.19 (d, *J* = 5.9 Hz, 1H), 7.73 – 7.64 (m, 6H), 7.46 (t, *J* = 7.7 Hz, 2H), 7.34 (t, *J* = 7.4 Hz, 1H), 6.81 (d, *J* = 5.9 Hz, 1H).

4.1.1.4. 2-chloro-*N*-(4'-chloro-[1,1'-biphenyl]-4-yl)pyrimidin-4-amine (**2d**). Yield: 0.082 g, 40%). ¹H NMR (600 MHz, CDCl₃) δ 8.16 (d, *J* = 5.9 Hz, 1H), 7.62 – 7.57 (m, 2H), 7.53 – 7.49 (m, 2H), 7.44 – 7.39 (m, 4H), 7.01 (s, 1H), 6.65 (d, *J* = 5.9 Hz, 1H).

4.1.1.5. 2-chloro-*N*-(3'-chloro-[1,1'-biphenyl]-4-yl)pyrimidin-4-amine (**2e**). Yield: 0.206 g, 86%. ¹H NMR (500 MHz, CDCl₃) δ 8.17 (d, *J* = 5.9 Hz, 1H), 7.60 (d, *J* = 8.7 Hz, 2H), 7.47 – 7.41 (m, 4H), 7.40 – 7.36 (m, 2H), 7.13 (s, 1H), 6.67 (d, *J* = 5.9 Hz, 1H).

4.1.1.6. 2-chloro-*N*-(4'-methyl-[1,1'-biphenyl]-4-yl)pyrimidin-4-amine (**2f**). Yield: 0.069 g, 21%. ¹H NMR (500 MHz, CDCl₃) δ 8.15 (d, *J* = 5.8 Hz, 1H), 7.64 – 7.59 (m, 2H), 7.50 – 7.47 (m, 2H), 7.39 – 7.35 (m, 2H), 7.29 – 7.25 (m, 2H, signal overlapping with CDCl₃), 7.00 (s, 1H), 6.65 (d, *J* = 5.9 Hz, 1H), 2.41 (s, 3H).

4.1.2. General procedure for synthesis of compounds **3a-v**. To a solution of alkyl amine (1.0 mmol) and DIPEA (1.6 mmol) in *n*-butanol (1 mL), the corresponding monosubstituted pyrimidine (0.4 mmol) was added. The mixture was stirred and heated at 190 °C in a sealed vial, and the reaction progress was monitored by TLC. The reaction solution was poured into water and extracted with dichloromethane. The organic layer was sequentially washed with brine, dried over anhydrous Na₂SO₄ and

concentrated in *vacuo*. The crude product was purified by column chromatography (SiO₂, dichloromethane/methanol).

4.1.2.1. *N*⁴-(4-chlorophenyl)-*N*²-(2-(morpholin-4-yl)ethyl)pyrimidine-2,4-diamine (**3a**). Yield: 0.028 g, 25%. ¹H NMR (600 MHz, CDCl₃) δ 7.94 (d, *J* = 5.7 Hz, 1H), 7.36 (d, *J* = 8.7 Hz, 2H), 7.32 – 7.28 (m, 2H), 6.56 (br s, 1H), 5.98 (d, *J* = 5.7 Hz, 1H), 5.36 (br s, 1H), 3.74 – 3.70 (m, 4H), 3.49 (q, *J* = 5.7 Hz, 2H), 2.59 (t, *J* = 6.1 Hz, 2H), 2.49 (br s, 4H). ¹³C NMR (151 MHz, CDCl₃) δ 162.0, 161.0, 157.0, 137.4, 129.2, 128.9, 122.7, 95.2, 67.0, 57.3, 53.4, 37.7. HR-MS (ES) calcd for C₁₆H₂₁ClN₅O [M+1]⁺ 334.1435, found 334.1434.

4.1.2.2. *N*²-(2-morpholinoethyl)-*N*⁴-(*p*-tolyl)pyrimidine-2,4-diamine (**3b**). Yield: 0.013 g, 21%. ¹H NMR (500 MHz, CDCl₃) δ 7.89 (d, *J* = 5.8 Hz, 1H), 7.22 (d, *J* = 8.1 Hz, 2H), 7.15 (d, *J* = 8.1 Hz, 2H), 6.61 (br s, 1H), 5.99 (d, *J* = 5.8 Hz, 1H), 5.55 (br s, 1H), 3.71 (t, *J* = 4.6 Hz, 4H), 3.48 (q, *J* = 5.8 Hz, 2H), 2.57 (t, *J* = 6.2 Hz, 2H), 2.48 (br s, 4H), 2.33 (s, 3H). ¹³C NMR (126 MHz, CDCl₃) δ 162.1, 161.7, 156.7, 135.9, 134.2, 129.8, 122.5, 94.6, 67.0, 57.4, 53.4, 37.7, 20.9. HR-MS (ES) calcd for C₁₇H₂₄N₅O [M+1]⁺ 314.1981, found 314.1984.

4.1.2.3. *N*⁴-((1,1'-biphenyl)-4-yl)-*N*²-(2-(morpholin-4-yl)ethyl)pyrimidine-2,4-diamine (**3c**). Yield: 0.020 g, 26%. ¹H NMR (600 MHz, CDCl₃) δ 7.97 (d, *J* = 5.8 Hz, 1H), 7.60 – 7.56 (m, 4H), 7.47 – 7.42 (m, 4H), 7.36 – 7.31 (m, 1H), 6.58 (s, 1H), 6.08 (d, *J* = 5.8 Hz, 1H), 5.46 (br s, 1H), 3.72 (t, *J* = 4.6 Hz, 4H), 3.52 (q, *J* = 5.8 Hz, 2H), 2.60 (t, *J* = 6.2 Hz, 2H), 2.50 (m, 4H). ¹³C NMR (151 MHz, CDCl₃) δ 162.4, 161.3, 157.5, 140.6, 138.3, 129.0, 128.0, 127.2, 126.9, 121.9, 67.1, 57.5, 53.6, 37.9. HR-MS (ES) calcd for C₂₂H₂₆N₅O [M+1]⁺ 376.2137, found 376.2140.

4.1.2.4. *N*⁴-(4'-methyl-[1,1'-biphenyl]-4-yl)-*N*²-(2-morpholinoethyl)pyrimidine-2,4-diamine (**3d**). Yield: 0.0145 g, 56 ¹H NMR (600 MHz, CDCl₃) δ 7.94 (d, *J* = 5.8 Hz,

1H), 7.56 (d, $J = 8.2$ Hz, 2H), 7.48 (d, $J = 7.8$ Hz, 2H), 7.43 (d, $J = 8.1$ Hz, 2H), 7.25 (d, $J = 7.6$ Hz, 2H), 6.71 (s, 1H), 6.07 (d, $J = 5.8$ Hz, 1H), 5.61 (br s, 1H), 3.72 (t, $J = 4.6$ Hz, 4H), 3.51 (q, $J = 5.8$ Hz, 2H), 2.60 (t, $J = 6.1$ Hz, 2H), 2.49 (t, $J = 4.4$ Hz, 4H), 2.39 (s, 3H). ^{13}C NMR (151 MHz, CDCl_3) δ 162.2, 161.4, 157.0, 137.9, 137.7, 137.1, 137.0, 129.7, 127.7, 126.8, 122.1, 95.2, 67.1, 57.5, 53.6, 37.9, 21.2. HR-MS (ES) calcd for $\text{C}_{23}\text{H}_{27}\text{N}_5\text{O}$ $[\text{M}+\text{H}]^+$ 390.2294, found 390.2302; $[\text{M}+\text{Na}]^+$: 412.2113, found: 412.2113.

4.1.2.5. N^4 -([1,1'-biphenyl]-4-yl)- N^2 -(2-(piperidin-1-yl)ethyl)pyrimidine-2,4-diamine (**3e**). Yield: 0.025 g, 36%. ^1H NMR (600 MHz, CDCl_3) δ 7.95 (d, $J = 5.6$ Hz, 1H), 7.60 – 7.55 (m, 4H), 7.48 – 7.41 (m, 4H), 7.33 (t, $J = 7.3$ Hz, 1H), 6.82 (br s, 1H), 6.09 (d, $J = 5.7$ Hz, 1H), 5.64 (br s, 1H), 3.55 (q, $J = 5.6$ Hz, 2H), 2.63 (t, $J = 6.1$ Hz, 2H), 2.51 (br s, 4H), 1.66 – 1.61 (m, 4H), 1.46 (br s, 2H). ^{13}C NMR (151 MHz, CDCl_3) δ 162.3, 161.3, 157.2, 140.6, 138.4, 136.8, 128.9, 127.9, 127.2, 126.9, 121.9, 95.3, 57.7, 54.5, 38.2, 25.7, 24.3. HR-MS (ES) calcd for $\text{C}_{23}\text{H}_{28}\text{N}_5$ $[\text{M}+1]^+$ 374.2345, found 374.2322.

4.1.2.6. N^4 -(4'-chloro-[1,1'-biphenyl]-4-yl)- N^2 -(2-(piperidin-1-yl)ethyl)pyrimidine-2,4-diamine (**3f**). Yield: 0.014 g, 34%. ^1H NMR (600 MHz, CDCl_3) δ 7.96 (d, $J = 5.8$ Hz, 1H), 7.53 (d, $J = 8.6$ Hz, 2H), 7.50 (d, $J = 8.5$ Hz, 2H), 7.47 (d, $J = 8.3$ Hz, 2H), 7.40 (d, $J = 8.5$ Hz, 2H), 6.68 (s, 1H), 6.06 (d, $J = 5.8$ Hz, 1H), 5.65 (s, 1H), 3.52 (q, $J = 5.8$ Hz, 2H), 2.60 (t, $J = 6.2$ Hz, 2H), 2.47 (s, 4H), 1.61 (p, $J = 5.6$ Hz, 4H), 1.45 (br s, 2H). ^{13}C NMR (151 MHz, CDCl_3) δ 162.3, 161.2, 157.3, 139.1, 138.7, 135.4, 133.3, 129.1, 128.1, 127.8, 121.8, 57.7, 54.5, 38.3, 25.9, 24.4. HR-MS (ES) calcd for $\text{C}_{23}\text{H}_{26}\text{ClN}_5$ $[\text{M}+\text{H}]^+$ 408.1955, found: 408,1955.

4.1.2.7. N^4 -(4-chlorophenyl)- N^2 -(2,2,6,6-tetramethylpiperidin-4-yl)pyrimidine-2,4-diamine (**3g**). Yield: 0.0304 g, 41%. ^1H NMR (500 MHz, CDCl_3) δ 7.92 (d, $J = 5.6$ Hz, 1H), 7.44 (d, $J = 8.3$ Hz, 2H), 7.27 (m, 1H), 7.25 (m, 1H), 6.51 (s, 1H), 5.93 (d, $J = 5.7$ Hz, 1H), 4.81 (br s, 1H), 4.35 – 4.25 (m, 1H), 2.03 (dd, $J = 12.7, 3.7$ Hz, 2H), 1.31 (s,

6H), 1.16 (s, 6H), 0.98 (t, $J = 12.2$ Hz, 2H). ^{13}C NMR (151 MHz, CDCl_3) δ 161.8, 161.0, 157.5, 137.9, 129.2, 128.6, 122.2, 95.7, 51.5, 45.8, 43.9, 35.0, 28.8. HR-MS (ES) calcd for $\text{C}_{19}\text{H}_{26}\text{ClN}_5$ $[\text{M}+\text{H}]^+$ 360.1955, found 360.1951.

4.1.2.8. N^4 -([1,1'-biphenyl]-4-yl)- N^2 -(2,2,6,6-tetramethylpiperidin-4-yl)pyrimidine-2,4-diamine (**3h**). Yield: 0.026 g, 16%. ^1H NMR (600 MHz, CDCl_3) δ 7.94 (d, $J = 5.6$ Hz, 1H), 7.57 – 7.55 (m, 6H), 7.44 (t, $J = 7.9$ Hz, 2H), 7.33 (t, $J = 7.4$ Hz, 1H), 6.70 (br s, 1H), 6.02 (d, $J = 5.6$ Hz, 1H), 4.94 (br s, 1H), 4.40 – 4.31 (m, 1H), 2.06 (dd, $J = 12.6$, 3.7 Hz, 2H), 1.34 (s, 6H), 1.18 (s, 6H), 1.05 (d, $J = 12.0$ Hz, 2H). ^{13}C NMR (151 MHz, CDCl_3) δ 161.8, 161.2, 157.2, 140.7, 138.5, 136.6, 129.0, 127.8, 127.2, 126.9, 121.5, 95.7, 51.7, 45.6, 43.8, 34.9, 28.6. HR-MS (ES) calcd for $\text{C}_{25}\text{H}_{31}\text{N}_5$ $[\text{M}+\text{H}]^+$ 402.2658, found 402.2658.

4.1.2.9. N^4 -(4'-chloro-[1,1'-biphenyl]-4-yl)- N^2 -(2,2,6,6-tetramethylpiperidin-4-yl)pyrimidine-2,4-diamine (**3i**). Yield: 0.0035 g, 6%. ^1H NMR (600 MHz, CDCl_3) δ 7.90 (d, $J = 5.4$ Hz, 1H), 7.55 (d, $J = 8.5$ Hz, 2H), 7.50 (d, $J = 8.3$ Hz, 2H), 7.48 (d, $J = 8.4$ Hz, 2H), 7.41 – 7.39 (m, 2H), 6.75 (br s, 1H), 6.01 (d, $J = 5.7$ Hz, 1H), 4.39-4.33 (m, 1H), 2.05 (d, $J = 3.7$ Hz, 1H), 2.03 (s, 2H), 1.38 (s, 6H), 1.23 (s, 6H), 1.16 (t, $J = 12.2$ Hz, 2H). ^{13}C NMR (151 MHz, CDCl_3) δ 161.3, 161.2, 139.0, 138.6, 135.4, 133.3, 129.1, 128.1, 127.7, 121.5, 95.8, 52.5, 45.0, 43.6, 34.2, 29.8, 28.1. HR-MS (ES) calcd for $\text{C}_{25}\text{H}_{30}\text{ClN}_5$ $[\text{M}+\text{H}]^+$: 436.2268, found 436.2266; $[\text{M}+\text{Na}]^+$: 458.2087, found: 458.2091

4.1.2.10. N^4 -(3'-chloro-[1,1'-biphenyl]-4-yl)- N^2 -(2,2,6,6-tetramethylpiperidin-4-yl)pyrimidine-2,4-diamine (**3j**). Yield: 0.0150 g, 11%. ^1H NMR (600 MHz, CDCl_3) δ 7.93 (d, $J = 5.4$ Hz, 1H), 7.57 – 7.50 (m, 5H), 7.45 – 7.41 (m, 1H), 7.36 (t, $J = 7.8$ Hz, 1H), 7.31 (dq, $J = 8.0$, 1.0 Hz, 1H), 6.66 (br s, 1H), 6.02 (d, $J = 5.5$ Hz, 1H), 5.21 (br s, 1H), 4.38 – 4.33 (m, 1H), 2.08 – 2.03 (m, 2H), 1.39 (s, 6H), 1.25 (s, 6H), 1.18 – 1.14

(m, 2H). ^{13}C NMR (151 MHz, CDCl_3) δ 161.5, 161.1, 142.5, 139.0, 135.1, 134.9, 130.2, 127.9, 127.2, 127.0, 125.0, 123.1, 121.4, 95.8, 45.0, 43.6, 34.2, 29.8, 28.1. HR-MS (ES) calcd for $\text{C}_{25}\text{H}_{31}\text{ClN}_5$ $[\text{M}+\text{H}]^+$ 436.2268, found 436.2279.

4.1.2.11. N^4 -(4'-methyl-[1,1'-biphenyl]-4-yl)- N^2 -(2,2,6,6-tetramethylpiperidin-4-yl)pyrimidine-2,4-diamine (**3k**). Yield: 0.0062 g, 11%. ^1H NMR (600 MHz, CDCl_3) δ 7.91 (d, $J = 5.6$ Hz, 1H), 7.54-7.52 (m, 4H), 7.46 (d, $J = 7.8$ Hz, 2H), 7.25 (d, $J = 7.8$ Hz, 2H), 6.60 (br s, 1H), 6.01 (d, $J = 5.7$ Hz, 1H), 5.14 (br s, 1H), 4.38-4.32 (m, 1H), 2.40 (s, 3H), 2.06 (d, $J = 3.7$ Hz, 1H), 2.04 (d, $J = 3.5$ Hz, 2H), 1.34 (s, 6H), 1.26 (s, 6H), 1.05 (t, $J = 12.0$ Hz, 2H). ^{13}C NMR. HR-MS (ES) calcd for $\text{C}_{26}\text{H}_{33}\text{N}_5$ $[\text{M}+\text{H}]^+$ 416.2814, found 416.2818.

4.1.2.12. N^4 -(4-chlorophenyl)- N^2 -((pyridin-3-yl)methyl)pyrimidine-2,4-diamine (**3l**). Yield: 0.016 g, 26%. ^1H NMR (600 MHz, CDCl_3) δ 8.62 (s, 1H), 8.52 (d, $J = 4.0$ Hz, 1H), 7.97 (d, $J = 5.7$ Hz, 1H), 7.68 (d, $J = 7.8$ Hz, 1H), 7.29 – 7.24 (m, 5H, signal overlapping with CDCl_3), 6.44 (s, 1H), 6.01 (d, $J = 5.8$ Hz, 1H), 5.35 (br s, 1H), 4.64 (d, $J = 6.0$ Hz, 2H). ^{13}C NMR (151 MHz, CDCl_3) δ 162.2, 161.1, 157.6, 149.2, 148.8, 137.4, 135.2, 135.1, 129.3, 125.8, 123.6, 122.9, 43.1. HR-MS (ES) calcd for $\text{C}_{16}\text{H}_{15}\text{ClN}_5$ $[\text{M}+1]^+$ 312.1016, found 312.1018.

4.1.2.13. N^4 -([1,1'-biphenyl]-4-yl)- N^2 -(pyridin-3-ylmethyl)pyrimidine-2,4-diamine (**3m**). Yield: 0.024 g, 27%. ^1H NMR (500 MHz, $\text{DMSO}-d_6$) δ 9.29 (s, 1H), 8.57 (s, 1H), 8.42 (dd, $J = 4.70, 1.5$ Hz, 1H), 7.88 (d, $J = 5.7$ Hz, 1H), 7.74 (d, $J = 7.8$ Hz, 1H), 7.63 – 7.61 (m, 3H), 7.53 (d, $J = 6.5$ Hz, 2H), 7.45 – 7.42 (m, 3H), 7.34 – 7.29 (m, 2H), 6.05 (d, $J = 5.6$ Hz, 1H), 4.51 (d, $J = 6.2$ Hz, 2H). ^{13}C NMR (126 MHz, CDCl_3) δ 158.3, 154.3, 151.6, 140.9, 140.5, 135.1, 133.4, 128.9, 128.8, 128.7, 127.6, 127.4, 127.2, 126.9, 126.7, 121.4, 104.9, 43.8. HR-MS (ES) calcd for $\text{C}_{22}\text{H}_{20}\text{N}_5$ $[\text{M}+1]^+$ 354.1719, found 354.1722.

4.1.2.14. N^4 -(4'-chloro-[1,1'-biphenyl]-4-yl)- N^2 -(pyridin-3-ylmethyl)pyrimidine-2,4-diamine (**3n**). Yield: 0.010 g, 21%. ^1H NMR (500 MHz, DMSO- d_6) δ 9.33 (s, 1H), 8.58 (s, 1H), 8.43 (dd, $J = 4.7, 1.6$ Hz, 1H), 7.89 (d, $J = 5.7$ Hz, 1H), 7.77 – 7.73 (m, 1H), 7.68 – 7.65 (m, 2H), 7.58 – 7.44 (m, 5 H), 7.36 – 7.33 (m, 1H), 6.06 (d, $J = 5.6$ Hz, 1H), 4.52 (d, $J = 6.2$ Hz, 2H). ^{13}C NMR (151 MHz, DMSO- d_6) δ 161.7, 160.4, 160.4, 156.2, 148.6, 147.6, 140.2, 138.7, 138.6, 136.1, 134.6, 131.6, 131.4, 128.7, 127.7, 126.6, 123.3, 123.2, 119.5, 41.9. HR-MS (ES) calcd for $\text{C}_{22}\text{H}_{18}\text{ClN}_5$ $[\text{M}+\text{H}]^+$ 388.1329, found 388.1325

4.1.2.15. N^4 -(3'-chloro-[1,1'-biphenyl]-4-yl)- N^2 -(pyridin-3-ylmethyl)pyrimidine-2,4-diamine (**3o**). Yield: 0.013 g, 21%. ^1H NMR (600 MHz, CDCl_3) δ 8.64 (br s, 1H), 8.52 (d, $J = 4.6$ Hz, 1H), 7.99 (d, $J = 5.8$ Hz, 1H), 7.71 (d, $J = 7.8$ Hz, 1H), 7.57 – 7.54 (m, 1H), 7.52 (d, $J = 8.4$ Hz, 2H), 7.45 (d, $J = 7.9$ Hz, 1H), 7.42 (d, $J = 8.5$ Hz, 2H), 7.36 (t, $J = 7.9$ Hz, 1H), 7.30 (d, $J = 7.9$ Hz, 1H), 7.28 – 7.24 (m, 1H, signal overlapping with CDCl_3), 6.58 (s, 1H), 6.11 (d, $J = 5.7$ Hz, 1H), 5.40 (br s, 1H), 4.66 (d, $J = 6.1$ Hz, 2H). ^{13}C NMR (151 MHz, CDCl_3) δ 171.8, 161.1, 157.3, 149.1, 148.6, 142.3, 138.5, 135.3, 135.1, 135.0, 134.7, 130.0, 127.8, 127.1, 126.9, 124.9, 123.4, 122.0, 121.7, 43.0. HR-MS (ES) calcd for $\text{C}_{22}\text{H}_{19}\text{ClN}_5$ $[\text{M}+1]^+$ 388.1329, found 388.1329.

4.1.2.16. 3-(((4-([1,1'-biphenyl]-4-ylamino)pyrimidin-2-yl)amino)methyl)pyridine 1-oxide (**3p**). Yield: 0.0071 g, 26%. ^1H NMR (600 MHz, CDCl_3) δ 8.31 (s, 1H), 8.11 (d, $J = 6.3$ Hz, 1H), 7.93 (d, $J = 5.8$ Hz, 1H), 7.59 – 7.53 (m, 4H), 7.44 (t, $J = 7.6$ Hz, 2H), 7.39 (d, $J = 8.2$ Hz, 2H), 7.34 (t, $J = 7.4$ Hz, 1H), 7.28 (d, $J = 8.0$ Hz, 1H), 7.22 (t, $J = 6.4$ Hz, 1H), 6.84 (s, 1H), 6.14 (d, $J = 5.8$ Hz, 1H), 5.65 (br s, 1H), 4.60 (d, $J = 6.2$ Hz, 2H). ^{13}C NMR (151 MHz, CDCl_3) δ 162.0, 161.9, 161.4, 157.2, 140.5, 140.0, 138.5, 137.9, 137.8, 137.2, 129.0, 127.9, 127.3, 127.0, 125.8, 125.2, 122.2, 42.4. HR-MS (ES) calcd for $\text{C}_{22}\text{H}_{20}\text{N}_5\text{O}$ $[\text{M}+1]^+$ 370.1668, found 370.1679.

4.1.2.17. *N*-([1,1'-biphenyl]-4-yl)-2-(4-methylpiperazin-1-yl)pyrimidin-4-amine (**3q**). Yield: 0.019 g, 22%. ¹H NMR (500 MHz, CDCl₃) δ 8.01 (d, *J* = 5.7 Hz, 1H), 7.60 – 7.56 (m, 4H), 7.46 – 7.41 (m, 4H), 7.33 (t, *J* = 7.4 Hz, 1H), 6.59 (br s, 1H), 6.05 (d, *J* = 5.7 Hz, 1H), 3.85 (t, *J* = 5.1 Hz, 4H), 2.50 (t, *J* = 5.1 Hz, 4H), 2.35 (s, 3H). ¹³C NMR (151 MHz, CDCl₃) δ 161.9, 161.0, 157.3, 140.6, 138.4, 136.7, 128.9, 127.9, 127.2, 126.9, 121.7, 95.0, 55.1, 46.3, 43.8. HR-MS (ES) calcd for C₂₁H₂₄N₅ [M+1]⁺ 346.2032, found 346.2151.

4.1.2.18. *N*-(4'-chloro-[1,1'-biphenyl]-4-yl)-2-(4-methylpiperazin-1-yl)pyrimidin-4-amine (**3r**). Yield: 0.0039 g, 23%. ¹H NMR (600 MHz, CDCl₃) δ 8.02 (d, *J* = 5.7 Hz, 1H), 7.55 – 7.52 (m, 2H), 7.52 – 7.50 (m, 2H), 7.47 – 7.44 (m, 2H), 7.41 – 7.39 (m, 2H), 6.54 (br s, 1H), 6.03 (d, *J* = 5.7 Hz, 1H), 3.86 – 3.81 (m, 3H), 2.49 (t, *J* = 5.1 Hz, 4H), 2.35 (s, 3H). ¹³C NMR (151 MHz, CDCl₃) δ 161.9, 160.8, 157.4, 139.1, 138.8, 135.3, 133.3, 129.1, 128.1, 127.7, 121.6, 95.1, 55.1, 46.4, 43.9, 29.8. HR-MS (ES) calcd for C₂₁H₂₂ClN₅ [M+H]⁺ 380.1642, found 380.1634.

4.1.2.19. *N*-(3'-chloro-[1,1'-biphenyl]-4-yl)-2-(4-methylpiperazin-1-yl)pyrimidin-4-amine (**3s**). Yield: 0.0296 g, 49%. ¹H NMR (600 MHz, CDCl₃) δ 8.03 (d, *J* = 5.7 Hz, 1H), 7.58 – 7.52 (m, 3H), 7.49 – 7.44 (m, 3H), 7.36 (t, *J* = 7.8 Hz, 1H), 7.30 (dq, *J* = 7.9, 1.0 Hz, 1H), 6.61 (br s, 1H), 6.03 (d, *J* = 5.7 Hz, 1H), 3.84 (t, *J* = 4.5 Hz, 4H), 2.48 (t, *J* = 5.0 Hz, 4H), 2.34 (s, 3H). ¹³C NMR (151 MHz, CDCl₃) δ 161.9, 160.8, 157.3, 142.5, 139.0, 135.0, 134.8, 130.2, 128.9, 127.9, 127.2, 127.0, 126.9, 125.0, 121.5, 95.1, 55.1, 46.4, 43.9. HR-MS (ES) calcd for C₂₁H₂₃ClN₅ [M+H]⁺ 380.1642, found 380.1629.

4.1.2.20. *N*-(4'-methyl-[1,1'-biphenyl]-4-yl)-2-(4-methylpiperazin-1-yl)pyrimidin-4-amine (**3t**). Yield: 0.0117 g, 49%. ¹H NMR (600 MHz, CDCl₃) δ 8.01 (d, *J* = 5.7 Hz, 1H), 7.57 – 7.55 (m, 2H), 7.49 – 7.47 (m, 2H), 7.43 – 7.41 (m, 2H), 7.26 – 7.24 (m, 2H), 6.50 (br s, 1H), 6.04 (d, *J* = 5.7 Hz, 1H), 3.84 (t, *J* = 5.2 Hz, 4H), 2.50 (t, *J* = 5.2 Hz,

4H), 2.40 (s, 3H), 2.35 (s, 3H). ^{13}C NMR (151 MHz, CDCl_3) δ 161.9, 161.0, 157.3, 138.1, 137.7, 137.0, 136.7, 129.7, 127.7, 126.8, 121.8, 94.9, 55.2, 46.4, 43.8, 29.8. HR-MS (ES) calcd for $\text{C}_{22}\text{H}_{25}\text{N}_5$ $[\text{M}+\text{H}]^+$ 360.2188, found 360.2188; $[\text{M}+\text{Na}]^+$ 382.2008, found: 382.1991

4.1.2.21. 2-(4-(4-((4-chlorophenyl)amino)pyrimidin-2-yl)piperazin-1-yl)ethan-1-ol (**3u**). Yield: 0.020 g, 30%. ^1H NMR (500 MHz, CDCl_3) δ 8.00 (d, $J = 5.7$ Hz, 1H), 7.34 – 7.26 (m, 4H), 6.49 (br s, 1H), 5.95 (d, $J = 5.7$ Hz, 1H), 3.80 (t, $J = 5.0$ Hz, 4H), 3.66 (t, $J = 5.3$ Hz, 2H), 2.60 – 2.55 (m, 6H). ^{13}C NMR (126 MHz, CDCl_3) δ 161.8, 160.8, 157.4, 137.7, 129.3, 128.8, 122.7, 95.0, 59.6, 57.9, 53.0, 44.0. HR-MS (ES) calcd for $\text{C}_{16}\text{H}_{21}\text{ClN}_5\text{O}$ $[\text{M}+1]^+$ 334.1435, found 334.1488.

4.1.2.22. 2-(4-(4-(((1,1'-biphenyl)-4-yl)amino)pyrimidin-2-yl)piperazin-1-yl)ethan-1-ol (**3v**). Yield: 0.017 g, 25%. ^1H NMR (600 MHz, CDCl_3) δ 8.02 (d, $J = 5.7$ Hz, 1H), 7.60 – 7.56 (m, 4H), 7.47 – 7.41 (m, 4H), 7.33 (t, $J = 7.4$ Hz, 1H), 6.72 (s, 1H), 6.05 (d, $J = 5.7$ Hz, 1H), 3.84 (t, $J = 4.9$ Hz, 4H), 3.68 (t, $J = 5.2$ Hz, 2H), 2.61 – 2.56 (m, 7H). ^{13}C NMR (151 MHz, CDCl_3) δ 161.9, 161.0, 157.3, 140.6, 138.3, 136.8, 129.0, 127.9, 127.2, 126.9, 121.8, 95.0, 59.6, 57.9, 53.0, 43.9. HR-MS (ES) calcd for $\text{C}_{22}\text{H}_{26}\text{N}_5\text{O}$ $[\text{M}+1]^+$ 376.2137, found 376.2143.

4.1.3. General procedure for the synthesis of compounds **4a-d**. DIPEA was added (3.6 mmol) to a round-bottom flask containing a mixture of 2,4-dichloropyrimidine (**1**) (3.3 mmol) and the corresponding amine (3.3 mmol) in ethanol (10 mL) at 0°C . The reaction mixture was stirred for 5 minutes at 0°C and then refluxed at 90°C overnight. The solvent was evaporated in vacuo. The residue was re-dissolved in a mixture of ethyl acetate and dichloromethane and washed with a NaHCO_3 solution and brine. The aqueous layer was washed with ethyl acetate. The combined organic layer was dried

over anhydrous Na_2SO_4 and concentrated in vacuo. The products were obtained as solids, which were recrystallized from ethanol.

4.1.3.1. 2-chloro-*N*-(4-chlorobenzyl)pyrimidin-4-amine (**4a**). Yield: 0.7436 g, 87%. ^1H NMR (600 MHz, CDCl_3) δ 8.03 (d, $J = 5.4$ Hz, 1H), 7.33 (d, $J = 8.4$ Hz, 2H), 7.25 (d, $J = 8.3$ Hz, 2H), 6.23 (d, $J = 5.6$ Hz, 1H), 5.72 (br s, 1H), 4.53 (br s, 2H).

4.1.3.2. 2-chloro-*N*-(4-fluorobenzyl)pyrimidin-4-amine (**4b**). Yield: 0.5438 g, 68%. ^1H NMR (600 MHz, CDCl_3) δ 8.03 (d, $J = 4.6$ Hz, 1H), 7.31 – 7.27 (m, 2H), 7.05 (d, $J = 8.5$ Hz, 2H), 6.23 (d, $J = 5.7$ Hz, 1H), 5.37 (br s, 1H), 4.53 (br s, 2H).

4.1.3.3. 2-chloro-*N*-(4-methylbenzyl)pyrimidin-4-amine (**4c**). Yield: 0.5744 g, 73%. ^1H NMR (600 MHz, CDCl_3) δ 8.00 (s, 1H), 7.20 (d, $J = 7.8$ Hz, 2H), 7.17 (d, $J = 7.9$ Hz, 2H), 6.23 (d, $J = 6.0$ Hz, 1H), 5.27 (br s, 1H), 4.49 (br s, 2H), 2.34 (s, 3H).

4.1.3.4. 2-chloro-*N*-(4-methoxybenzyl)pyrimidin-4-amine (**4d**). Yield: 0.3732 g, 56%. ^1H NMR (600 MHz, CDCl_3) δ 8.01 (s, 1H), 7.23 (d, $J = 8.4$ Hz, 2H), 6.89 (d, $J = 8.6$ Hz, 2H), 6.23 (d, $J = 6.1$ Hz, 1H), 5.22 (br s, 1H), 4.46 (br s, 2H), 3.80 (s, 3H).

4.1.4. General procedure for the synthesis of compounds **5a-e**. Compounds **5a-e** were synthesized as described before for compounds **3a-v**.

4.1.4.1 N^4 -(4-chlorobenzyl)- N^2 -(pyridin-3-ylmethyl)pyrimidine-2,4-diamine (**5a**). Yield: 0.150 g, 39%. ^1H NMR (600 MHz, CDCl_3) δ 8.58 (s, 1H), 8.49 (d, $J = 3.7$ Hz, 1H), 7.84 (d, $J = 5.3$ Hz, 1H), 7.62 (d, $J = 7.0$ Hz, 1H), 7.28 – 7.26 (m, 2H, signal overlapping with CDCl_3), 7.23 – 7.18 (m, 3H), 5.74 (d, $J = 5.7$ Hz, 1H), 5.32 (br s, 1H), 4.98 (br s, 1H), 4.58 (d, $J = 5.9$ Hz, 2H), 4.47 (d, $J = 4.5$ Hz, 2H). ^{13}C NMR (151 MHz, CDCl_3) δ 163.0, 162.1, 156.4, 149.2, 148.5, 137.3, 135.5, 135.2, 133.2, 128.9, 128.8, 123.5, 44.4, 42.9. HR-MS (ES) calcd for $\text{C}_{17}\text{H}_{17}\text{ClN}_5$ $[\text{M}+\text{H}]^+$ 326.1172, found 326.1170.

4.1.4.2. N^4 -(4-chlorobenzyl)- N^2 -(2,2,6,6-tetramethylpiperidin-4-yl)pyrimidine-2,4-diamine (**5b**). Yield: 0.0228 g, 17%. ^1H NMR (600 MHz, CDCl_3) δ 7.81 (d, $J = 5.3$ Hz, 1H), 7.30 (d, $J = 8.1$ Hz, 2H), 7.24 (d, $J = 8.1$ Hz, 2H), 5.71 (d, $J = 5.6$ Hz, 1H), 4.97 (br s, 1H), 4.83 (br s, 1H), 4.53 (br s, 2H), 4.26 – 4.23 (m, 1H), 1.99 (dd, $J = 12.5, 3.2$ Hz, 2H), 1.26 (s, 6H), 1.20 (s, 6H), 1.08 (t, $J = 10.2$ Hz, 2H). ^{13}C NMR (151 MHz, CDCl_3) δ 163.0, 161.8, 156.6, 137.6, 133.3, 128.9, 128.8, 94.7, 51.9, 45.7, 43.8, 34.9, 28.5. HR-MS (ES) calcd for $\text{C}_{20}\text{H}_{29}\text{ClN}_5$ $[\text{M}+\text{H}]^+$ 374.2111, found 374.2144.

4.1.4.3. N^4 -(4-fluorobenzyl)- N^2 -(2,2,6,6-tetramethylpiperidin-4-yl)pyrimidine-2,4-diamine (**5c**). Yield: 0.0243 g, 16%. ^1H NMR (600 MHz, CDCl_3) δ 7.81 (d, $J = 5.6$ Hz, 1H), 7.31 – 7.26 (m, 2H, signal overlapping with CDCl_3), 7.04 – 6.96 (m, 2H), 5.70 (d, $J = 5.7$ Hz, 1H), 4.94 (br s, 1H), 4.82 (br s, 1H), 4.57 – 4.51 (m, 2H), 4.29 – 4.22 (m, 1H), 2.02 – 1.97 (m, 2H), 1.24 (s, 6H), 1.16 (s, 6H), 1.01 – 0.97 (m, 2H). ^{13}C NMR (151 MHz, CDCl_3) δ 162.9, 161.5, 129.0, 128.9, 115.6, 115.4, 115.3, 115.2, 51.8, 45.3, 44.5, 43.6, 34.6, 28.2. HR-MS (ES) calcd for $\text{C}_{20}\text{H}_{29}\text{FN}_5$ $[\text{M}+\text{H}]^+$ 358.2407, found 358.2420.

4.1.4.4. N^4 -(4-methylbenzyl)- N^2 -(2,2,6,6-tetramethylpiperidin-4-yl)pyrimidine-2,4-diamine (**5d**). Yield: 0.0243 g, 16%. ^1H NMR (600 MHz, CDCl_3) δ 7.76 (s, 1H), 7.23 – 7.18 (m, 2H), 7.16 – 7.10 (m, 2H), 5.70 (d, $J = 5.9$ Hz, 1H), 5.35 (br s, 1H), 5.01 (br s, 1H), 4.55 – 4.50 (m, 2H), 4.30 – 4.24 (m, 1H), 2.33 (d, $J = 9.0$ Hz, 3H), 1.99 (dd, $J = 12.5, 3.6$ Hz, 2H), 1.24 (d, $J = 4.7$ Hz, 6H), 1.18 (d, $J = 5.4$ Hz, 6H), 1.07 – 1.02 (m, 2H). ^{13}C NMR (151 MHz, CDCl_3) δ 144.7, 137.3, 136.7, 129.5, 129.3, 127.6, 125.1, 54.4, 52.2, 45.1, 43.6, 34.4, 28.1, 21.2. HR-MS (ES) calcd for $\text{C}_{21}\text{H}_{32}\text{N}_5$ $[\text{M}+\text{H}]^+$ 354.2658, found 354.2673.

4.1.4.5. N^4 -(4-methoxybenzyl)- N^2 -(2,2,6,6-tetramethylpiperidin-4-yl)pyrimidine-2,4-diamine (**5e**). Yield: 0.055 g, 35%. ^1H NMR (600 MHz, CDCl_3) δ 7.78 (br s, 1H), 7.24 (d, $J = 8.6$ Hz, 2H), 6.88 (d, $J = 8.7$ Hz, 2H), 5.71 (d, $J = 5.9$ Hz, 1H), 4.92 (br s, 1H),

4.48 (br s, 2H), 4.33 – 4.27 (m, 1H), 3.80 (s, 3H), 2.02 (dd, $J = 12.6, 3.4$ Hz, 2H), 1.29 (br s, 6H), 1.21 (br s, 6H), 0.90 – 0.83 (m, 2H). ^{13}C NMR (151 MHz, CDCl_3) δ 164.2, 163.0, 161.8, 159.2, 156.5, 155.4, 128.9, 114.2, 55.5, 51.5, 45.8, 43.8, 35.1, 29.9, 28.6. HR-MS (ES) calcd for $\text{C}_{21}\text{H}_{32}\text{N}_5\text{O}$ $[\text{M}+\text{H}]^+$ 370.2607, found 370.2633.

4.1.5. 2-chloro-4-hydrazinylpyrimidine (**6**). A mixture of 2,4-dichloropyrimidine (**1**) (70 mmol) and TEA (70 mmol) in methanol (5 mL) was cooled to 0-5 °C in an ice bath. Hydrazine hydrate (80 mmol) was added slowly dropwise to the cold reaction. Then, the reaction mixture was allowed to stir at room temperature for 2 h. The solid obtained was filtered, washed with chilled water and dried under vacuum overnight to afford **6**. Yield: 0.4 g, 40%.

4.1.6. (*E*)-2-chloro-4-(2-(2,4-dichlorobenzylidene)hydrazinyl)pyrimidine (**7**). Compound **6** (0.76 mmol) was dissolved in EtOH (3 mL) and 2,4-dichlorobenzaldehyde (0.91 mol) was added to the mixture. The mixture was refluxed for 1 h and allowed to stand at room temperature. The solid was filtered, washed with EtOH and dried to afford compound **7**. Yield: 0.3 g, 100%. ^1H NMR (500 MHz, $\text{DMSO}-d_6$) δ 12.15 (s, 1H), 8.46 (s, 1H), 8.31 (d, $J = 5.8$ Hz, 1H), 8.10 (d, $J = 8.6$ Hz, 1H), 7.73 (d, $J = 2.1$ Hz, 1H), 7.51 (dd, $J = 8.6, 2.0$ Hz, 1H), 7.27 (s, 1H).

4.1.7. (*E*)-4-(2-(2,4-dichlorobenzylidene)hydrazinyl)-*N*-(2-morpholinoethyl)pyrimidin-2-amine (**8**). Compound **8** was synthesized as described before for compounds **3a-v**. Yield: 0.09 g, 3%. ^1H NMR (500 MHz, CDCl_3) δ 8.41 (br s, 1H), 8.11 – 8.06 (m, 2H), 7.98 (d, $J = 8.6$ Hz, 1H), 7.40 (d, $J = 2.0$ Hz, 1H), 7.28 (dd, $J = 8.6, 2.0$ Hz, 1H), 6.59 (d, $J = 5.7$ Hz, 1H), 5.57 (br s, 1H), 3.72 (t, $J = 4.6$ Hz, 4H), 3.49 – 3.44 (m, 3H), 2.59 (t, $J = 6.1$ Hz, 2H), 2.49 (s, 4H). ^{13}C NMR (151 MHz, CDCl_3) δ 161.9, 161.8, 157.8, 135.7, 133.9, 133.2, 130.5, 129.8, 127.9, 127.7, 67.1, 57.4, 53.6, 37.8. HR-MS (ES) calcd for $\text{C}_{17}\text{H}_{21}\text{Cl}_2\text{N}_6\text{O}$ $[\text{M}+\text{H}]^+$ 395.1154, found 395.1126.

4.1.8. 2-chloropyrimidine-4-amine (**9**). A suspension of 2,4-dichloropyrimidine (**1**) (4.0 mmol) in ammonium hydroxide (4.0 mmol) was stirred at 90°C for 5 h. The mixture was cooled to room temperature and a white solid precipitated. The solid was filtered out and washed with ethyl ether. Yield: 0.23 g, 45 %. ¹H NMR (600 MHz, CDCl₃) δ 8.16 (d, *J* = 5.2 Hz, 1H), 6.66 (d, *J* = 5.2 Hz, 1H), 5.21 (br s, 2H).

4.1.9. *N*-(2-chloropyrimidin-4-yl)-5-(pyridin-2-yl)thiophene-2-carboxamide (**10**). In a bottom flask purged with nitrogen, 5-(pyridin-2-yl)thiophene-2-carboxylic acid (0.24 mmol) was added in portions to a mixture of **9** (0.27 mmol), EDCI·HCl (0.27 mmol) and HOBt (0.12 mmol) in *N*-methylpyrrolidin-2-one (2 mL). The mixture was stirred at room temperature overnight. Water (10 mL) and ethyl acetate (10 mL) were added, and the mixture was stirred for 10 min. The mixture was partitioned, and the aqueous phase was extracted twice with ethyl acetate. The combined organic extracts were concentrated under vacuo. The product (**10**) was obtained after purification by preparative chromatography (SiO₂, dichloromethane:methanol). The yellow solid product was used in the next step without further purification. Yield: 0.0088 g, 11%.

4.1.10. *N*-(2-((2-morpholinoethyl)amino)pyrimidin-4-yl)-5-(pyridin-2-yl)thiophene-2-carboxamide (**11**). Compound **11** was synthesized as described before for compounds **3a-v**. Yield: 0.004 g, 36%. ¹H NMR (500 MHz, CDCl₃) δ 9.5, (s, 1H), 8.60 (d, *J* = 4.8 Hz, 1H), 7.75 – 7.64 (m, 3H), 7.57 (d, *J* = 3.9 Hz, 1H), 7.54 (d, *J* = 3.9 Hz, 2H), 7.22 (dd, *J* = 7.2, 6.3 Hz, 1H), 6.64 (br s, 1H), 3.75 (t, *J* = 4.6 Hz, 4H), 3.55 (q, *J* = 5.5 Hz, 2H), 2.60 (t, *J* = 5.9 Hz, 2H), 2.51 (t, *J* = 4.7 Hz, 4H). ¹³C NMR (151 MHz, CDCl₃) δ 162.0, 161.4, 151.9, 149.9, 148.6, 139.4, 137.0, 130.0, 124.8, 123.0, 119.3, 67.1, 57.1, 53.6, 29.9. HR-MS (ES) calcd for C₂₀H₂₂N₆O₂S [M+H]⁺ 411.1603,

4.1.11. *N*-([1,1'-biphenyl]-4-yl)-2-(2-morpholinoethoxy)pyrimidin-4-amine (**12**). A mixture of a NaH (0.46 mmol) and 4-(2-hydroxyethyl)morpholine (0.46 mmol) in THF

(1.5 mL) was stirred at 0°C. The reaction was allowed to warm at room temperature and stirred for 30 minutes. After this period, compound **2c** was added under nitrogen atmosphere, the vial was sealed and the mixture was stirred and heated at 80 °C overnight. The reaction solution was poured into water and extracted with dichloromethane. The organic layer was sequentially washed with brine, dried over anhydrous Na₂SO₄ and concentrated in vacuo. The crude product was purified by column chromatography (SiO₂, dichloromethane/methanol). Yield: 0.0171 g, 25%. ¹H NMR (600 MHz, CDCl₃) δ 8.10 (d, *J* = 5.8 Hz, 1H), 7.61 – 7.56 (m, 4H), 7.47 – 7.41 (m, 4H), 7.35 (t, *J* = 7.4 Hz, 1H), 7.15 (br s, 1H), 6.40 (d, *J* = 5.8 Hz, 1H), 4.47 (t, *J* = 5.7 Hz, 2H), 3.71 (t, *J* = 4.5 Hz, 4H), 2.79 (t, *J* = 5.9 Hz, 2H), 2.57 (br s, 4H). ¹³C NMR (151 MHz, CDCl₃) δ 165.2, 162.7, 158.1, 140.4, 137.8, 137.5, 129.0, 128.1, 127.4, 127.0, 122.7, 99.0, 67.1, 64.8, 57.5, 54.1. HR-MS (ES) calcd for C₂₂H₂₅N₄O₂ [M+H]⁺ 377.1978, found 377.1925.

4.2. Biological studies

4.2.1. Antiviral assay using DENV reporter

One day prior to infection, A549 or BHK-21 cells were seeded in a 24-well plate. The next day, cells were infected with luciferase reporter infectious DENV at MOI of 1 [36] in the absence or presence of compounds to be tested. Controls included uninfected cells, infected cells, and DMSO-treated infected cells. Prior to infection, the viral inoculum was incubated 30 min in the presence of each compound. The viral inoculum was removed from the cells 1 h later, and incubated with fresh medium containing the compound. Luciferase activity was measured at 8 h and 24 h postinfection p.i. using the Renilla luciferase assay system according to the manufacturer's protocol (Promega). These time points allow discrimination between early steps of viral infection (entry-

translation of incoming genome) up to 8 h and, genome RNA amplification, evident after 24 h of infection [19].

4.2.2. Cytotoxicity test

Cell viability was measured by two different assays: MTT and crystal violet (CV). Vero cell confluent cultures (African green monkey kidney, ATCC CCL-81) grown in Eagle's minimum essential medium (MEM) (Gibco™ Thermo Fisher Scientific, Carlsbad, CA) supplemented with 5% inactivated bovine serum were exposed for 48 h to serial twofold compound dilutions, three wells for each concentration, and then viability was tested. In the MTT method, 10 mL of MM containing MTT (final concentration 0.5 mg/mL) was added to each well. After 2 h of incubation, the supernatant was removed, ethanol was added to each well and absorbance was measured at 595 nm. For CV assay, cells were fixed with 10 % formaldehyde during 15 min. Then, cells were washed with water and stained with CV (0.05 % CV in 10 % ethanol) during 30 min. After washing, colourant was eluted with ethanol/acetic acid, 50/0.1% and absorbance was recorded at 590 nm [21]. The cytotoxic concentration 50% (CC_{50}) was calculated as the compound concentration required to reduce the absorbance signal by 50% compared to untreated controls.

4.2.3. Viral infection in cells and quantification of viral titers.

Virus stocks of DENV-1 (Hawaii), DENV-2 (New Guinea C), DENV-3 (H87) and DENV-4 (8124) were provided by Dr. A.S. Mistchenko (Hospital de Niños Dr. Ricardo Gutierrez, Buenos Aires, Argentina). All the stocks were prepared in C6/36 cells and titrated by a standard plaque assay in Vero cells. For plaque assay, 10-fold dilutions of samples containing virus were added to monolayers of confluent Vero cells at 37°C for 1 h. Following incubation, the inoculum was removed, and monolayers were overlaid with 1 mL of

MEM containing 1% methylcellulose. The cells were incubated at 37°C for 7 days and fixed using 4% formaldehyde. Finally, plaques were stained with 0.1% crystal violet in 20% ethanol.

4.2.4 Virus yield reduction assay Vero cells grown in 24 well plates were infected at m.o.i. 0.1 PFU/cell. After 1 h adsorption at 4°C, cells were washed and refed with maintenance medium containing or not serial two fold dilutions of each tested compound respectively. After 24 and 48 h of incubation at 37°C, supernatant cultures were harvested and extracellular virus yields were determined by a plaque assay. The effective concentration 50% (EC₅₀) was calculated as the concentration required to reduce virus yield by 50% in the compound treated cultures compared with untreated ones. All determinations were performed in triplicate.

4.2.5. Virus RNA synthesis. Cells were infected at a m.o.i. of 1. At 24 h p.i., extracellular medium was harvested to quantify virus production and cells were processed for real time RT-PCR assays. Total RNA was extracted by using TRIZOL (Invitrogen Life Technologies) according to the manufacturer's instructions. Then, cDNA was generated by using murine reverse transcriptase M-MLV (100 U/μL, Invitrogen) and random primers. This cDNA was amplified by real time PCR using SYBRGreen (Roche) detection. The mix reaction volume was 25 μl including 2 μL of cDNA, DNA polymerase GoTaq (5 U/μL, Promega) and specific primers to amplify all DENV serotypes: Sense 5' -TTGAGTAAACYRTGCTGCCTGTAGCTC-3' Antisense 5' -GGGTCTCCTCTAACCTCTAGTCCT-3'. Real time PCR was carried out with an initial incubation at 95°C during 2 min, followed by 35 cycles of 30 s at 95°C, 1 min at 58°C, and 1 min at 72°C and a final step of 10 min at 72°C. Amplification plots were analyzed with Opticon Monitor 3.1 software and the

comparative threshold cycle (Ct) method was used to determine gene expression relative to the cellular gene *β-actin*. Statistical analyses were performed using GraphPad Prism software. Comparison of means was tested by one - way analysis of variance (ANOVA) with Dunnett's posttest. Statistical significance was defined as $P < 0.05$ (95% confidence interval).

4.3. Molecular docking

Docking studies were performed on the β -OG binding site of the Dengue E protein (PDB ID 1OKE). The system was described in terms of dihedral coordinates using the ECEPP/3 force field [37] as implemented in the Internal Coordinates Mechanics (ICM) program (version 3.7-2c, MolSoft LLC, La Jolla, CA) [38], and prepared in a similar fashion as earlier works [23,39]: water molecules were deleted; hydrogen atoms were added to the receptor structure; Asp and Glu amino-acids were assigned a -1 negative charge, and Arg and Lys amino-acids a $+1$ charge. Histidine tautomers were selected based on the hydrogen bonding network. The rigid-receptor:flexible-ligand docking protocol as implemented in ICM was used. The receptor was represented by six potential energy maps. The six rigid degrees of freedom and torsion angles were considered flexible during the docking procedure, and subjected to a global energy minimization protocol within the field of the receptor using a Monte Carlo with minimization protocol [38,40].

4.4. Molecular dynamics

MD simulations were performed using Amber16 and AmberTools16 package [41] using the Amber99SB force field [42]. The system was solvated with the TIP3P water model in a truncated octahedric box, extending 10 \AA from the protein, and neutralized adding

sufficient Na^+ ions. Bond lengths were constrained using the SHAKE algorithm allowing a 2 fs time-step. Long-range electrostatics interactions were taken into account using the particle-mesh Ewald (PME) approach. The non bonded cut-off for Coulomb and Van der Waals interactions were both 8 Å. Energy minimization was conducted through the steepest-descent algorithm and then switched to conjugate gradient. Then an equilibration of the whole system was performed during 100 ps of NVT simulation followed by 400 ps of NPT simulation. Temperature was kept constant at 300 K using a Langevin thermostat [43] with a collision frequency of 2 ps. Constant pressure of 1 bar was applied in all directions with a pressure relaxation time of 1.0 ps. Binding free energy was estimated with the Molecular Mechanics/Generalized Born Surface Area (MM/GBSA) method, using the MMPBSA.py [44] module implemented in Amber analysis tools.

4.5. Shake-flask method for drug solubility testing

The shake-flask method was used as a reference assay [45–47]. Test compounds (1.0 mg) were weighed into 2 mL glass vial, and 1 mL of the medium (simulated gastric fluid (SGF), simulated intestinal fluid (SIF) and phosphate buffered saline solution (PBS)) was added. The vial contents were mixed at 1500 rpm at 37 °C for 24 h and then incubated at 37 °C for 24 h. The sample was filtered (0.2 µm, Sterile Acrodisc® 13, GelmanScience) before analysis with UV3600 UV-VIS-NIR Spectrophotometer. Calibration curves were obtained from compounds over a wide concentration range and were constructed by plotting absorbance of the compounds against the concentration. All compounds were test in triplicate.

4.6. SGF, SIF and PBS stability

Stock solutions of test compounds were prepared at a concentration of 10 mM in DMSO. The stock solution was diluted in acetonitrile to 1 mM. The reactions were

initiated by the addition of the test compounds to the medium (SGF, SIF and PBS) (final concentration: 50 μM). Samples were incubated in a shaking water bath at 37°C and conducted in triplicate. Samples (125 μL) were taken at 0, 15, 30, 60, 90, 120 min and 375 μL of acetonitrile containing the internal standard (warfarin) was added to quench the reaction. The samples were vortexed for 1 min and then centrifugated at 25°C for 15 min at 14000 rpm. The supernatant was collected, diluted in methanol:water (50:50) and analyzed by high performance liquid chromatography-mass spectrometry (HPLC-MS). The quantification was based on the peak area ratio of the test compound vs. the internal standard.

The HPLC-MS analysis was performed using a Waters Alliance e2695 system fitted with a Waters XBridge C18 (4.6 x 150 mm, 3.5 μm particle size, Waters Corporation, Milford, MA, USA), coupled to a Waters SQD2 single quadrupole mass spectrometer with an electrospray ionization (ESI) source. Gradient elution was utilized in the chromatographic separation method using 60% acetonitrile, 40% water, 0.1% acetic acid and 10 mM ammonium acetate (mobile phase A), 90% isopropanol, 10 % acetonitrile, 0.1% acetic acid and 10 mM ammonium acetate (mobile phase B), with the following program: 0-5 min 5% B; 5-13 min 5-95% B; 13-15 min 95%. The flow rate was constant at 0.3 mL min^{-1} . After each sample injection, the gradient was returned to its initial conditions in 12 min. The injection volume was 5 μL . The column temperature was 35°C. The mass spectrometer was operated in positive ion mode with a probe capillary voltage of 3.0 kV. The sampling cone voltage was set to 45.0 V. The source and desolvation gas temperatures were set at 150°C and 350°C, respectively. The nitrogen gas desolvation flow rate was 600 L h^{-1} and the cone gas flow rate was 10 L h^{-1} . The mass spectrometer was calibrated across the range of m/z 20–2023 with a sodium and cesium iodide solution. Data were acquired in scan mode with a scan duration of

0.2 sec, and in SIRmode with unit resolution. Data acquisition and processing were carried out using MassLynx, version 4.1 software.

4.7. Mouse plasma stability

Stock solutions of test compounds were prepared at a concentration of 10 mM in DMSO. The stock solution was diluted in DMSO to 1 mM. The mouse plasma was diluted to 80% with PBS. The reactions were initiated by the addition of the test compounds to the preheated plasma solution (final concentration: 50 μ M). Samples were incubated in a shaking water bath at 37 °C and conducted in triplicate. Samples (50 μ L) were taken at 0, 15, 30, 60, 90, 120 min and 200 μ L of cold acetonitrile containing the internal standard (warfarin) was added to deproteinize the plasma. The samples were vortexed for 1 min and then centrifugated at 4 °C for 15 min at 14000 rpm. Enalapril was used as positive control incubation. The supernatant was collected, diluted in methanol: water (50:50) and analyzed by HPLC-MS. The quantification was based on the peak area ratio of the test compound vs. the internal standard. The HPLC-MS analysis was performed as described before for SGF, SIF and PBS stability.

5. Acknowledgments

This work has been supported by the Agencia Nacional de Promoción Científica y Tecnológica, Argentina (*National Agency for Scientific and Technological Promotion*, ANPCYT, (PICT 2014-1884, PICT 2014-3599, PICT 2017-3767), Consejo Nacional de Investigaciones Científicas y Técnicas (*National Scientific and Technical Research Council*), CONICET, PUE 055, PIP 2014 11220130100721 and PIP11220170100171CO and Universidad de Buenos Aires (UBA) 20020160100091BA. LGG, MEM, CCG, AVG, CNC and MB are members of the Research Career CONICET. MV is a technical staff member from the CONICET, MLM

was supported by a doctoral fellowship from UBA. ESL, GAF, LB and MGA were supported by a fellowship from CONICET and NSA was supported by a doctoral fellowship by AMPCYT.

MB thanks William Jorgensen for providing an academic license for BOMB and QikProp software. CNC thanks Molsoft LLC for providing an academic license for the ICM program. Authors also wish to thank the Centro de Computación de Alto Rendimiento (*Computational Centre of High Performance Computing*, CeCAR) and the Centro de Cálculo de Alto Desempeño (Universidad Nacional de Córdoba) for granting the use of their computational resources.

6. Appendix A. Supplementary data

The Supporting Information contains synthesis of *N*-oxide(pyridin-3-yl)methanamine (**12**) and general procedure for the synthesis of biphenyls (**19a-19c**), figures S1-S12 and ¹H, ¹³C NMR spectral charts for compounds **3a-v**, **5a-e**, **8**, **11** and **12**

7. References

- [1] K. Wichapong, A. Nueangaudom, S. Pianwanit, W. Sippl, S. Kokpol, Identification of potential hit compounds for Dengue virus NS2B/NS3 protease inhibitors by combining virtual screening and binding free energy calculations, *Trop. Biomed.* 30 (2013) 388–408.
- [2] F.A. Murphy, Epidemiology of Human and Animal Viral Diseases, in: B.W.J. Mahy, M.H.V. Van Regenmortel (Eds.), *Encycl. Virol.* (Third Ed., Third Edit, Academic Press, Oxford, 2008: pp. 140–148. doi:10.1016/B978-012374410-4.00390-3.
- [3] B.L. Ligon, Dengue fever and dengue hemorrhagic fever: A review of the history, transmission, treatment, and prevention, *Semin. Pediatr. Infect. Dis.* 16 (2005) 60–65. doi:10.1053/j.spid.2004.09.013.
- [4] G.N. Malavige, S. Fernando, D.J. Fernando, S.L. Seneviratne, Dengue viral infections, *Postgrad. Med. J.* . 80 (2004) 588–601. doi:10.1136/pgmj.2004.019638.
- [5] D.J. Gubler, Epidemic dengue/dengue hemorrhagic fever as a public health, social and economic problem in the 21st century, *Trends Microbiol.* 10 (2002) 100–103. doi:10.1016/S0966-842X(01)02288-0.
- [6] S.S. Whitehead, J.E. Blaney, A.P. Durbin, B.R. Murphy, Prospects for a dengue virus vaccine, *Nat. Rev. Microbiol.* 5 (2007) 518–528. doi:10.1038/nrmicro1690.

- [7] [Http://www.sanofipasteur.com/en/](http://www.sanofipasteur.com/en/)., The data was updated in the Sanofi Pasteur official site:, (n.d.).
- [8] World Health Organization, Dengue vaccine: WHO position paper, July 2016 – recommendations, *Vaccine*. 35 (2017) 1200–1201. doi:<https://doi.org/10.1016/j.vaccine.2016.10.070>.
- [9] H. E Clapham, B. A Wills, Implementing a dengue vaccination programme-who, where and how?, *Trans. R. Soc. Trop. Med. Hyg.* 112 (2018) 367–368. doi:[10.1093/trstmh/try070](https://doi.org/10.1093/trstmh/try070).
- [10] S.P. Lim, Dengue drug discovery: Progress, challenges and outlook, *Antiviral Res.* 163 (2019) 156–178. doi:<https://doi.org/10.1016/j.antiviral.2018.12.016>.
- [11] A.K. Timiri, B.N. Sinha, V. Jayaprakash, Progress and prospects on DENV protease inhibitors, *Eur. J. Med. Chem.* 117 (2016) 125–143. doi:<https://doi.org/10.1016/j.ejmech.2016.04.008>.
- [12] R.J. Kuhn, W. Zhang, M.G. Rossmann, S. V Pletnev, J. Corver, E. Lenches, et al., Structure of Dengue Virus: Implications for Flavivirus Organization, Maturation, and Fusion, *Cell*. 108 (2002) 717–725. doi:[10.1016/S0092-8674\(02\)00660-8](https://doi.org/10.1016/S0092-8674(02)00660-8).
- [13] Y. Modis, S. Ogata, D. Clements, S.C. Harrison, A ligand-binding pocket in the dengue virus envelope glycoprotein, *Proc. Natl. Acad. Sci. U. S. A.* 100 (2003) 6986–6991. doi:[10.1073/pnas.0832193100](https://doi.org/10.1073/pnas.0832193100).
- [14] M. de Wispelaere, W. Lian, S. Potisopon, P.-C. Li, J. Jang, S.B. Ficarro, et al., Inhibition of Flaviviruses by Targeting a Conserved Pocket on the Viral Envelope Protein, *Cell Chem. Biol.* 25 (2018) 1006-1016.e8. doi:[10.1016/j.chembiol.2018.05.011](https://doi.org/10.1016/j.chembiol.2018.05.011).
- [15] Z. Zhou, M. Khaliq, J.-E. Suk, C. Patkar, L. Li, R.J. Kuhn, et al., Antiviral Compounds Discovered by Virtual Screening of Small-Molecule Libraries against Dengue Virus E Protein, *ACS Chem. Biol.* 3 (2008) 765–775. doi:[10.1021/cb800176t](https://doi.org/10.1021/cb800176t).
- [16] W.L. Jorgensen, M. Bollini, V. V. Thakur, R.A. Domaoal, K.A. Spasov, K.S. Anderson, Efficient discovery of potent anti-HIV agents targeting the Tyr181Cys variant of HIV reverse transcriptase, *J. Am. Chem. Soc.* 133 (2011) 15686–15696. doi:[10.1021/ja2058583](https://doi.org/10.1021/ja2058583).
- [17] A.H.F. Lee, E.T. Kool, Novel Benzopyrimidines as Widened Analogues of DNA Bases, *J. Org. Chem.* 70 (2005) 132–140. doi:[10.1021/jo0483973](https://doi.org/10.1021/jo0483973).
- [18] F. Kato, T. Hishiki, Dengue Virus Reporter Replicon is a Valuable Tool for Antiviral Drug Discovery and Analysis of Virus Replication Mechanisms, *Viruses*. 8 (2016) 122. doi:[10.3390/v8050122](https://doi.org/10.3390/v8050122).
- [19] J.A. Mondotte, P.-Y. Lozach, A. Amara, A. V Gamarnik, Essential Role of Dengue Virus Envelope Protein N Glycosylation at Asparagine-67 during Viral Propagation, *J. Virol.* . 81 (2007) 7136–7148. doi:[10.1128/JVI.00116-07](https://doi.org/10.1128/JVI.00116-07).
- [20] M.B. Mazzucco, L.B. Talarico, S. Vatansever, A.C. Carro, M.L. Fascio, N.B.

- D'Accorso, et al., Antiviral activity of an N-allyl acridone against dengue virus, *J. Biomed. Sci.* 22 (2015) 29. doi:10.1186/s12929-015-0134-2.
- [21] L.B. Talarico, C.A. Pujol, R.G.M. Zibetti, P.C.S. Faría, M.D. Nosedá, M.E.R. Duarte, et al., The antiviral activity of sulfated polysaccharides against dengue virus is dependent on virus serotype and host cell, *Antiviral Res.* 66 (2005) 103–110. doi:10.1016/j.antiviral.2005.02.001.
- [22] Y. Modis, S. Ogata, D. Clements, S.C. Harrison, Structure of the dengue virus envelope protein after membrane fusion, *Nature.* 427 (2004) 313–319. doi:10.1038/nature02165.
- [23] E.S. Leal, M.G. Aucar, L.G. Gebhard, N.G. Iglesias, M.J. Pascual, J.J. Casal, et al., Discovery of novel Dengue virus entry inhibitors via a structure-based approach, *Bioorg. Med. Chem. Lett.* 27 (2017) 3851–3855. doi:10.1016/j.bmcl.2017.06.049.
- [24] T. Kampmann, R. Yennamalli, P. Campbell, M.J. Stoermer, D.P. Fairlie, B. Kobe, et al., In silico screening of small molecule libraries using the dengue virus envelope E protein has identified compounds with antiviral activity against multiple flaviviruses, *Antiviral Res.* 84 (2009) 234–241. doi:10.1016/j.antiviral.2009.09.007.
- [25] M.K. Poh, A. Yip, S. Zhang, J.P. Priestle, N.L. Ma, J.M. Smit, et al., A small molecule fusion inhibitor of dengue virus, *Antiviral Res.* 84 (2009) 260–266. doi:10.1016/j.antiviral.2009.09.011.
- [26] A.G. Schmidt, K. Lee, P.L. Yang, S.C. Harrison, Small-molecule inhibitors of dengue-virus entry, *PLoS Pathog.* 8 (2012). doi:10.1371/journal.ppat.1002627.
- [27] Q.-Y. Wang, S.J. Patel, E. Vangrevelinghe, H.Y. Xu, R. Rao, D. Jaber, et al., A Small-Molecule Dengue Virus Entry Inhibitor, *Antimicrob. Agents Chemother.* 53 (2009) 1823–1831. doi:10.1128/AAC.01148-08.
- [28] Z. Zhou, M. Khaliq, J.E. Suk, C. Patkar, L. Li, R.J. Kuhn, et al., Antiviral compounds discovered by virtual screening of small-molecule libraries against dengue virus E protein, *ACS Chem. Biol.* 3 (2008) 765–775. doi:10.1021/cb800176t.
- [29] G. Barreiro, J.T. Kim, C.R.W. Guimarães, C.M. Bailey, R.A. Domaol, L. Wang, et al., From Docking False-Positive to Active Anti-HIV Agent, *J. Med. Chem.* 50 (2007) 5324–5329. doi:10.1021/jm070683u.
- [30] W.L. Jorgensen, P. Schyman, Treatment of Halogen Bonding in the OPLS-AA Force Field: Application to Potent Anti-HIV Agents, *J. Chem. Theory Comput.* 8 (2012) 3895–3901. doi:10.1021/ct300180w.
- [31] W.L. Jorgensen, J. Tirado-Rives, Molecular modeling of organic and biomolecular systems using BOSS and MCPRO, *J. Comput. Chem.* 26 (2005) 1689–1700. doi:10.1002/jcc.20297.
- [32] K.M. Frey, D. Puleo, K. a. Spasov, M. Bollini, W.L. Jorgensen, K.S. Anderson, Structure-based Evaluation of Non-nucleoside Inhibitors with Improved Potency and Solubility that Target HIV Reverse Transcriptase Variants, *J. Med. Chem.*

- (2015) 150220115749004. doi:10.1021/jm501908a.
- [33] W.L. Jorgensen, E.M. Duffy, Prediction of drug solubility from structure, *Adv. Drug Deliv. Rev.* 54 (2002) 355–366. doi:http://dx.doi.org/10.1016/S0169-409X(02)00008-X.
- [34] W.L. Jorgensen, Efficient drug lead discovery and optimization, *Acc. Chem. Res.* 42 (2009) 724–733. doi:10.1021/ar800236t.
- [35] W.L. Jorgensen, QikProp, v 3.0; Schrödinger LLC, (n.d.).
- [36] M.M. Samsa, J.A. Mondotte, J.J. Caramelo, A. V Gamarnik, Uncoupling cis-Acting RNA elements from coding sequences revealed a requirement of the N-terminal region of dengue virus capsid protein in virus particle formation., *J. Virol.* 86 (2012) 1046–58. doi:10.1128/JVI.05431-11.
- [37] G. Nemethy, K.D. Gibson, K.A. Palmer, C.N. Yoon, M.G. Paterlini, A. Zagari, et al., Energy parameters in polypeptides. 10. Improved geometrical parameters and nonbonded interactions for use in the ECEPP/3 algorithm, with application to proline-containing peptides, *J. Phys. Chem.* 96 (1992) 6472–6484.
- [38] R. Abagyan, M. Totrov, D. Kuznetsov, ICM - a New Method For Protein Modeling and Design - Applications to Docking and Structure Prediction From the Distorted Native Conformation, *J. Comput. Chem.* 15 (1994) 488–506.
- [39] M. Bollini, E.S. Leal, N.S. Adler, M.G. Aucar, G.A. Fernández, M.J. Pascual, et al., Discovery of Novel Bovine Viral Diarrhea Inhibitors Using Structure-Based Virtual Screening on the Envelope Protein E2, *Front. Chem.* 6 (2018) 79. doi:10.3389/fchem.2018.00079.
- [40] C.N. Cavasotto, M.G. Aucar, N.S. Adler, Computational chemistry in drug lead discovery and design, *Int. J. Quantum Chem.* 119 (2019) e25678. doi:10.1002/qua.25678.
- [41] D.A. Case, R.M. Betz, D.S. Cerutti, T.E. Cheatham, III, T.A. Darden, R.E. Duke, et al., AMBER 2016, University of California, San Francisco, (2016).
- [42] V. Hornak, R. Abel, A. Okur, B. Strockbine, A. Roitberg, C. Simmerling, Comparison of multiple Amber force fields and development of improved protein backbone parameters, *Proteins.* 65 (2006) 712–725. doi:10.1002/prot.21123.
- [43] R.L. Davidchack, R. Handel, M. V Tretyakov, Langevin thermostat for rigid body dynamics, *J. Chem. Phys.* 130 (2009) 234101. doi:10.1063/1.3149788.
- [44] B.R. Miller, T.D. McGee, J.M. Swails, N. Homeyer, H. Gohlke, A.E. Roitberg, MMPBSA.py: An Efficient Program for End-State Free Energy Calculations, *J. Chem. Theory Comput.* 8 (2012) 3314–3321. doi:10.1021/ct300418h.
- [45] C. Lipinski, Aqueous Solubility in Discovery, Chemistry, and Assay Changes, in: Wiley-VCH Verlag GmbH, Weinheim, 2003: pp. 215–131.
- [46] M. Bollini, K.M. Frey, J.A. Cisneros, K.A. Spasov, K. Das, J.D. Bauman, et al., Extension into the entrance channel of HIV-1 reverse transcriptase--crystallography and enhanced solubility., *Bioorg. Med. Chem. Lett.* 23 (2013)

5209–12. doi:10.1016/j.bmcl.2013.06.093.

- [47] M. Bollini, J. a Cisneros, K. a Spasov, K.S. Anderson, W.L. Jorgensen, Optimization of diarylazines as anti-HIV agents with dramatically enhanced solubility., *Bioorg. Med. Chem. Lett.* 23 (2013) 5213–6. doi:10.1016/j.bmcl.2013.06.091.

Journal Pre-proof

Highlights

- De novo design approach was used to identify new compounds against DENV E protein
- Lead Optimization was performed via molecular dynamics
- Several compounds displayed excellent potency against DENV
- Compounds 3e and 3h were potent compounds of all four sero-types of DENV
- 3e and 3h showed acceptable in vitro pharmacokinetics profile.

Journal Pre-proof